The Middle Pleistocene hominin mandible from Payre (Ardèche, France)

Christine Verna[a, b,*], Florent Détroit [a], Kornelius Kupczik[c], Julie Arnaud[d], Antoine Balzeau[a], Dominique Grimaud-Hervé[a], Simone Bertrand[e], Bernard Riou[f], Marie-Hélène Moncel[a].

[a] UMR 7194 CNRS/MNHN-Département Homme Environnement, Musée de l'Homme,17 Place du Trocadéro, 75016, Paris, France

[b] Department of Human Evolution, Max Planck Institute for Evolutionary Anthropology, Deutscher Platz 6, 04103, Leipzig, Germany.

[c] Max Planck Weizmann Center for Integrative Archaeology and Anthropology, Max Planck Institute for Evolutionary Anthropology, Deutscher Platz 6, 04103, Leipzig, Germany.

[d] Department of Humanities, Section of Prehistorical and Anthropological Sciences, University of Ferrara, C.so Ercole I d'Este 32, 44121 Ferrara

[e] Rondette, 07250, Rompon, France

[f] Muséum de l'Ardèche La Croizette 07120 Balazuc

** Corresponding author*

Email Address: christine.verna@mnhn.fr

The Middle Pleistocene hominin mandible from Payre (Ardèche, France)

Abstract

Although Neandertals are the best-known fossil hominins, the tempo and evolutionary processes in their lineage are strongly debated. This is in part due to the scarcity of the fossil record, in particular before the MIS 5. In 2010, a partial hominin mandible was discovered at the Middle Paleolithic site of Payre (France) in a layer that is dated to the end of MIS 8/beginning of MIS 7, a time period for which very few fossils are known in Europe. The Payre 15 mandible retains the complete symphyseal region and right lateral corpus with heavily worn P_4, M_1 and M_2 in situ. Taphonomic modifications in the form of three notches suggest that this individual was chewed by a carnivore. We provide here the first detailed description of this specimen and a comparative analysis that includes morphological features, linear mandibular dimensions, an elliptic Fourier analysis of the symphysis and a morphometric analysis of the M_1 roots (based on segmented CT-scan data). Our comparative sample encompasses European Middle and Upper Pleistocene specimens attributed to *Homo heidelbergensis* and *Homo neanderthalensis*, Upper Pleistocene and Holocene *Homo sapiens*. The Payre 15 mandible shows a combination of primitive and Neandertal-like features, with a receding symphyseal profile without any element of the mentum osseum, a posterior location of the mental foramen and lateral prominence. Its mandibular body is tall and thick anteriorly. Payre 15 has mesotaurodont M_1 roots and a three-rooted M2. By its dimensions and combination of features, Payre 15 aligns better with Middle Pleistocene European hominins than with MIS 6-3 Neandertals. Noteworthy, it falls well within the range of variation of the Sima de los Huesos sample. Our results underscore that the total pattern of Neandertal derived morphology was not achieved at the beginning of the MIS 7 and suggest a low level of mandibular diachronic changes for the period MIS 11-7.

Keywords

Early Middle Paleolithic; Neandertal; symphysis; Elliptic Fourier Analysis; tooth root

1.0 Introduction

Although there is a general agreement that Neandertals represent a hominin lineage rooted in Western Eurasia during the Middle Pleistocene, the tempo and mode of evolution in this lineage are the subjects of intense debates, which rely on both paleoanthropological and genetic data. These discussions have focused primarily on the divergence time of the H*omo sapiens* and H*omo neanderthalensis* lineages, as well as on the taxonomy and phylogeny of the late Middle Pleistocene European hominins (e.g. Arsuaga et al., 1997; Rosas and Bermúdez de Castro, 1997; Weaver et al., 2008; Hublin, 2009; Mounier et al., 2009; Endicott et al., 2010; Harvati et al., 2010; Stringer, 2012; Gómez-Robles et al., 2013; Prüfer et al., 2014; Bermudez de Castro et al., 2016, 2018; Manzi, 2016; Daura et al., 2017; Hanegraef et al., 2018; Roksandic et al., 2018; Zanolli, et al., 2018; Rosas et al., 2019; Gómez-Robles, 2019). Additionally, and in relation to the above-mentioned debates, the evolutionary processes underlying the establishment of the Neandertal morphology are also the subject of discussions and various models have been proposed (see Rosas et al., 2019 for a review). The first one, known as the accretion model (Dean et al., 1998; Hublin, 1998), emphasizes a gradual, cumulative and mosaic pattern of craniofacial changes in the European fossil record between the Marine Isotopic Stage (MIS) 15 and 4 that is best explained by genetic drift (Hublin, 1998; Weaver et al., 2007; Weaver, 2009). Alternative models have recently questioned the gradual and mosaic pattern of the process, suggesting instead some rapid changes involving two chronologically successive speciation events (Rosas et al., 2006), or the co-existence of more than one hominin lineage in Middle Pleistocene Europe (Arsuaga et

al., 2014; Bermudez de Castro et al., 2018) possibly reflecting repeated migrations from a "source population" in Southwestern Asia (Dennell et al., 2011; Bermudez de Castro et al., 2016, 2018; Hanegraef et al., 2018;Vialet et al, 2018).

Part of the difficulty in evaluating these models lies into the discontinuity of the Middle Pleistocene fossil record. In particular, very few fossils have been discovered for the period covering MIS 8-6. In 2010, a hominin mandibular fragment was found at the site of Payre in 2010 (Ardèche, France) in an archaeological layer that is attributed to the end of MIS 8/beginning of MIS 7 (see below). Here, we present the first detailed description and comparative analysis of this hominin mandible, with the goal to characterize its morphology and assess its taxonomy and biological affinities. We report on its dimensions, the morphology of its symphysis and lateral body, including an Elliptic Fourier Analysis of its symphyseal outline, as well as on the size and form of the first molar roots. By focussing on how this fossil hominin compares to European Middle and Late Pleistocene fossil specimens, we also aim to discuss how this new discovery contributes to the debates on the Early evolutionary history of the Neandertal lineage.

1.1 Context of the Payre 15 mandible

Located in the Rhône Valley (SE France) (Fig. 1), the site of Payre is now a rock shelter, which formed from a collapsed cave at the end of the MIS 6. Within the ~5m deep stratigraphic sequence, eight levels of Palaeolithic occupation were identified and classified into four stratigraphic Units including levels for Units G (Ga, Gb) and F (Fa to Fd) (Fig. 2). The sequence ranges from MIS 8 to the end of MIS 6 / beginning of MIS 5 based on ESR-U-series, TL, and TIMS (Grün et al., 2008; Valladas et al. 2008). The whole sequence lies on a thick stalagmitic

floor dated to 229 ky +-2 – 291 ky +- 3 by U-series-TIMS. The levels Gb and Ga (unit G) are dated by TL to 247 ky +-29 (arithmetic mean).

Biostratigraphic data confirm the radiometric dates with recurrent human occupations during temperate events (Moncel, 2008). The fauna is mainly composed of herbivores *Equus ferus, Stephanorhinus kirchbergensis, Stephanorhinus hemitoechus, Elephas, Bos primigenius, Hemitragus bonali, Cervus elaphus, Capreolus capreolus, Castor fiber*, *Ursus spelaeus,* and carnivores *Panthera leo spelaea, Cuon priscus, Felis silvestris, Lynx lynx, Vulpes vulpes* (Moncel, 2008). Faunal remains attest to similar human activities along the sequence and indicate hunting on cervids, equids, and bovids, and rhinoceros and elephants were probably scavenged (Patou-Mathis et al., in Moncel, 2008; Daujeard and Moncel, 2010; Daujeard et al., 2011; Moncel and Daujeard, 2012). Zooarcheological analysis indicates successive short-term seasonal occupations (Rivals et al., 2009; Daujeard and Moncel, 2010; Moncel and Daujeard, 2012). Bones were intensively broken, and some were burned.

Carnivores also inhabited the site, in particular bears (*Ursus spelaeus* mainly) that died during hibernation, as attested by disturbed but complete skeletons of young and adult bears in unit F especially (levels Fd to Fa), suggesting that hominid occupation alternated with carnivore denning at this site. Carnivores were more numerous in unit F than Unit G (levels Ga and Gb) suggesting a more intense human occupation during Unit G. Isotope analyses on both a human tooth and animals remains indicate a stable subsistence strategy over time and the use of local resources with resource partitioning visible between carnivores and humans (Ecker et al., 2013; Bocherens et al., 2016; Moncel et al., 2019). The lithic assemblages are attributed to the Early Middle Paleolithic (Chacon Navarro et al., 2016; Baena et al., 2017; Carmignani et al., 2017), flint being the main raw material used together with other local

stones. The core technology is mostly discoidal and orthogonal and the retouched artifacts are scrapers and points (Moncel, 2008; Moncel et al., 2009). Some large tools (bifaces, bifacial scrapers, simple scrapers) are made on quartzite, limestone and basalt pebbles or large flakes. Micro-wear studies attest the diversity of activities on the site (Hardy and Moncel, 2011). There are indications of fire in each level and an ashy lens was discovered at the top of level Ga without clear hearth structure (see details in Moncel, 2008).

Thirteen isolated hominin teeth and a parietal fragment were found throughout the sequence between 1994 and 2002, most of them coming from the basal levels Ga, and grouped in a small area (Moncel and Condemi, 2007). They were attributed to the Neandertal lineage (Condemi in Moncel, 2008). In June 2010, a hominin mandible (Fig. 3) was discovered in level Ga, close to the teeth and the parietal in the main chamber of the cave (Supplemental online Materials (SOM) Fig. S1). Following the order of discovery of these remains, this mandible is numbered Payre 15 (SOM Table S1), and its morphology is described here for the first time.

2. Material and methods

2.1 Computed tomography and symmetry-based virtual reconstruction of Payre 15

In 2010, the mandible was CT-scanned at the Pitié-Salpétrière Hospital in Paris (voxel size 0.16x0.16x0.34 mm) and the following year, it was micro-CT scanned again at the AST-RX platform in Paris with a voxel size of 57µm. Using these high-resolution data, the mandible was segmented in order to virtually remove the sediment as well as to distinguish the dental tissues (enamel, dentine, cement). Based on these segmented data (Fig. 4), we virtually reconstructed the mandible following the principle of bilateral symmetry. We first mirrored the preserved right hemi-mandible into a virtual left partial mandible. The two

objects were then aligned using the tool for manual alignment in Geomagic Studio® 2012. The alignment procedure was repeated three times to obtain a more accurate reconstruction. Seven landmarks were selected on both objects along the mid-sagittal section of the mandible. Based on these points the two objects were aligned and then fused together. Areas that were bilaterally present were removed from the left (mirrored) hemi mandible to obtain a 3D reconstruction of the mandible with a complete mandibular corpus (SOM Fig. S2). We proceeded three times to this virtual reconstruction. This virtual reconstruction allowed us to estimate the width of the mandible (see below).

2.2 Comparative samples

Given the chronological and individual age of the specimen, our comparative samples include primarily Middle and Late Pleistocene hominin samples (adult individuals) attributed to the Neandertal and *H. sapiens* lineages. European samples used in our analyses are MIS 7 to 3 Neandertals and Pre-MIS 9 European Middle Pleistocene specimens (MPH) that were commonly attributed to *H. heidelbergensis* (SOM Table S2), although considerable debate surrounds the taxonomy of these specimens (see below). The Neandertal sample includes specimens belonging to the MIS 7 to 3 from Europe and South-Western Asia, divided into Early (MIS 7-5e) and Late (MIS 5d-3) Neandertals (hereafter EN and LN respectively). Among the EN sample, two specimens are attributed to MIS 7 and are thus chronologically close to Payre 15, namely the mandible from Montmaurin-La-Niche (Vialet et al., 2018) and Ehringsdorf F (Street et al., 2006). The MPH sample includes data for mandibles from the sites of Arago, Mala Balanica (Roksandic et al., 2011; Skinner et al., 2016), Mauer (Rosas and Bermúdez de Castro, 1997) and Sima de los Huesos (Rosas, 2001). Despite the most recent and convincing morphological and genetic evidence that the Sima de los Huesos sample may belong to the Neandertal species (Martinón-Torres et al., 2012; Stringer, 2012;

Arsuaga et al., 2014; Meyer et al., 2016), the chronological gap (ca 200 ka) between these fossils, the Payre 15 mandible and the rest of the Neandertal sample led us to keep them in a "Pre-MIS 9 European Middle Pleistocene hominins" category. They are thus grouped together with fossil specimens from Arago, Mauer and Mala Balanica, despite the current debates regarding their taxonomy and the hypothesis that these fossils may represent more than one species (see above). In our view, further work needs to be done before achieving a resolution of these questions and before being able to securely assign each of these specimens to a specific taxon.

Our Pleistocene *H. sapiens* sample (EMH) includes MIS 5-4 African and South-West Asian Pleistocene specimens as well as MIS 3-2 European Upper Palaeolithic specimens. Finally, two comparative samples of recent humans (RMH) were used in the Elliptic Fourier Analysis (EFA) of the symphyseal profile as well as in the analysis of the size and form of the roots. The detailed composition of the samples used for the morphological and morphometric analyses are given in the (SOM Table S2).

2.3 Morphological features

A set of six discrete morphological features were scored and compared to their frequency distribution in the comparative samples. These features were scored following the criteria detailed in Dobson and Trinkaus (2002), and Rosas (2001): number and location of mental foramina (below an alveolus or an interdental septum); location of the lateral prominence; mylohyoid line orientation and location following Rosas (2001); and development of the mentum osseum, following Dobson and Trinkaus (2002). In the comparative material, the features were scored on both sides when preserved. The data come from our study of original specimens, supplemented by high quality casts as well as a few data from the literature (SOM Table S2). Frequency tables were then computed for

comparison (Table 1). For specimens that exhibit bilateral asymmetry, traits were scored as 0.5 for each side. In addition, frequencies for several combinations of features were tabulated, using a binomial scoring system based on the combination of features observed on Payre 15 as follow: mental foramen single vs. multiple; mental foramen below/posterior vs. anterior to the M_1 socket; lateral prominence below vs. anterior to the M_3 socket; mylohyoid line crossing the body in a diagonal vs. parallel way; mylohyoid line in a low vs. medium/high position. In this case, when both sides were preserved, each trait was recorded as present when observed on at least on one side.

2.4 Linear mandibular dimensions

Given the state of preservation of Payre 15, metric analyses include uni- and multivariate analyses of the following linear dimensions of the mandibular body: its height and breadth at the symphysis (HS, ES; M69, Martin and Saller, 1957) and along the lateral body below the P_4, M_1 and M_2 alveoli. Each measurement was taken three times and the mean value is given in the Table 2. In addition, external bi-M_2 width (largest distance between the alveolar borders, taken perpendicular to the median plane) was measured on the virtual reconstruction of Payre 15. Robusticity indices (Breadth x 100 / Height of the body) were also computed and included in our analyses. 2D linear dimensions were obtained on our study of original specimens and high quality casts with a few additional data from the literature (SOM Table S2).

Univariate analyses were carried out using adjusted z-scores (Azs; Scolan et al., 2012), in which 95% of the variation of the reference population is included between –1 and +1. An Azs value lower than –1 or higher than +1 is, therefore, outside 95% of the variation of the reference population.

In addition, two types of Principal Components Analyses (PCA) were performed on five linear dimensions measured in Payre 15 (Height and breadth at the symphysis and at the M_1, bi-M_2 width). First, a PCA was performed on the raw dimensions, then a between-group PCA (bgPCA) was performed on the same dimensions standardized for size using Log Shape Ratios (LSRs), in order to better distinguish shape differences from absolute size differences (Darroch and Mosimann, 1985; Jungers et al., 1995). In both analyses, Payre was projected as a supplementary individual.

2.5 Elliptic Fourier analysis of the symphyseal profile

For Elliptic Fourier Analysis (EFA), 3D models obtained with a Nextengine laser surface scanner were used. The scanning procedure, optimized for resolution (Arnaud et al., 2015), was applied to original specimens when available or otherwise to high-quality casts (see SOM Table S2). Three landmarks and 41 semi-landmarks were digitized along the outline of the symphysis profile. The three landmarks correspond to the infradentale (ld1), the intersection of the digastric fossae (ld2) and the infradentale posterior (ld3). Intra-observer error was tested on a random selection of eight specimens digitized ten times with a time interval of 24 hours. We calculated the deviation of each landmark to the centroid for each specimen separately, and then a mean error was calculated (Singleton, 2002; Lili et al., 2009). We obtained 4.6 % for ld1, 0.7 % for ld2 and 4.6% ld3.

Raw Cartesian coordinates were pre-processed in three steps. Three-dimensional coordinates were reduced to two-dimensions through a PCA (i.e. the scores of the first two principal components become the new coordinates of the landmarks and semi-landmarks). Since the sagittal plane of the symphysis is difficult to define virtually, we chose this specific protocol to reproduce a plane which is homologous in all our samples and close to the real sagittal plane. In a second step, the 41 semilandmarks were re-sampled equidistantly along the

curve. Finally, the new outlines were registered for size and orientation with a Procrustes superimposition on the three landmarks (Corny and Détroit, 2014).

Finally, the new dataset containing the normalized two-dimensional coordinates of the outlines (Procrustes residuals) were submitted to an elliptic Fourier analysis (EFA). This method, developed for the analysis of complex outlines, transforms outlines in a series of ellipses which become more complex and closer to the original outlines as the number of calculated coefficients (harmonics described by four Fourier descriptors) increase (Kuhl and Giardina, 1982; Lestrel, 1989, 1997). In our case, the Fourier descriptors of the nine first harmonics that account for 99% of the cumulative power (Lestrel, 1997), were retained and analyzed with a PCA in order to explore the variation calculated by the EFA.

Landmarks and semi-landmarks were digitized on 3D models using Landmark (IDAV Visualization and Graphics Research Group). Pre-processing of the data, Procrustes registration, EFA and PCA were performed in R (R Core Team, 2017), using the packages Momocs and Geomorph (Adams et al., 2017; Bonhomme et al., 2014) and functions adapted from Claude (2008).

2.6 First molar root size and form

From the 3D surface reconstruction of the lower M_1 root the following measurements were taken: cervical plane area, root surface area (both in mm^2), root length (mm), root stem and apex volume (both in mm^3). A PCA based on the correlation matrix of these variables was used to explore the overall variation in root size in the comparative sample (see SOM Table S2). In addition, M_1 root surface area of Payre 15 was compared to the comparative sample, while the bivariate association between M_1 root surface area and cervical plane area was assessed using reduced major axis regression (RMA). We also computed a volumetric bifurcation index (in %) as [(root stem volume / (root stem volume + root branch volume)) x

100] for the M_1 roots. The Payre 15 M_1 root was thus classified into one of the four groups: cynotaurodont: 0-24.9%, hypotaurodont- : 25-49.9%, mesotaurodont: 50-74.9% or hypertaurodont IV: 75-100% (see Kupczik and Hublin, 2010).

3. Description of Payre 15

3.1 State of preservation

Payre 15 is a mandibular fragment which retains the complete symphyseal region, the right lateral corpus from the socket of the left I_2 to the right M_3, and a very small portion of the inferior part of the ramus (Fig. 3). The corpus is almost intact up to the M_2-M_3 interalveolar septum. It is broken behind this point and the breakage passes through the M_3 socket. The ramus is represented by a horizontal band that extends behind this breakage and is ca 5 cm long and less than 2 cm high. The lower border is damaged so that the gonial angle is not preserved.

The incisors, the right canine, and the third premolar are missing post-mortem. Their alveolar sockets are filled with sediment. The right P_4 and M_1 are in situ, and their roots and crowns (albeit heavily worn) are preserved. At the time of the discovery of the mandible, the roots of the right M_2 were preserved but the crown was broken off at the cervix just above the bifurcation of the mesial and distal roots. In 2010, a sample was drilled into the M_2 for DNA analysis, removing a large part of its roots (Fig. 4). This sampling was done after the medical CT-scan acquisition but prior to microCT scanning (see above).

Some highly indurate sediment is still adhering to the bone and fills in particular entirely the sockets of the anterior teeth (SOM Fig. S3), although some sediment was

mechanically removed previously (this remaining sediment was however virtually removed during the segmentation process; Fig.4).

The P_4 and M_1 are heavily worn (stage 5 of Molnar, 1971) and their occlusal surface is almost entirely constituted by dentine (Fig. 5). The crown of the M_1 is partially broken and some enamel is lacking on its disto-buccal part. On both teeth, the plane of occlusal attrition slopes strongly towards the buccal side, reflecting a reversed Curve of Monson plane of occlusion (Osborn, 1982) at M_1. In addition, the M_1 shows a second plane of wear which is downward and distally oriented. On the P_4, some enamel is preserved on the lingual side as a ring along the lingual border and a small disto-lingual area. Lingually, the enamel ring is interrupted in the middle and slightly thicker on the distal side. The smooth morphology of the edges suggests that this interruption is not a fracture but is due to wear. A small secondary dentine patch is present at the center of the occlusal surface. On the M_1, the enamel is only preserved on the lingual side of the occlusal surface as a mesio-distal ring (that does not reach the disto-lingual corner of the crown) and as a small area retained between the location of the two lingual cusps.

Overall, when free of sediment, the bone surface of the mandible is well preserved. Some corrosion pitting is visible but remains minimal. No cut-marks were observed. Anteriorly, once virtually cleaned of the infilling sediment, one can see that the incisors sockets are well preserved and these teeth were likely lost post-mortem. The P_3 socket however sustained some taphonomic damage of its external margin.

Anteriorly, the breakage of the corpus has a straight outline and follows an oblique axis from the left I_2 alveolus to the inferior border below the right I_1 alveolus, next to the interdigastric spine. The broken edge is partly covered by concretions and its morphology

(roughened texture and right angle with the bone surface) clearly shows that it is ancient and of post-depositional origin. One large subvertical crack and several other thin cracks in the junction area between the corpus and the ramus can also be attributed to post-depositional taphonomic processes (probably due to sedimentary compression and/or weathering). Posteriorly, the broken edges of the fragment (at the level of the ramus) are not straight but show an irregular aspect. On the lateral aspect, two notches that expose spongy bone are noteworthy. One is ca 4 mm wide and is located on the inferior border, close to the posterior border of the fragment (SOM Fig. S4a). The second one is ca 3 mm wide and located on the upper margin of the fragment, at the junction between the corpus and the ramus (SOM Fig. S4b). Both notches show a rounded shape on the external table and are covered by concretions, which show that they are ancient. Finally, on the inner side, the breakage of the corpus below the M_3 socket also reveals a notch, aligned with an oblique fracture plane towards the inner side and a rather smooth surface (SOM Fig. S5). The overall shape and dimensions of these notches and the morphology of the associated fractures suggest breakage inflicted on fresh bone and although not fully diagnostic, these notches recall carnivore marks, probably from a large-size species.

3.2 Symphyseal region

The symphyseal profile is markedly receding (the symphysis is retreating relative to the alveolar plane) and its anterior surface is essentially flat, showing only a slight posteroinferior rounding of its anterior part. The anterior symphyseal surface is evenly rounded mediolaterally, and there is no element of a *mentum osseum* (no trace of *tuber symphyseos*, *mental fossa*, lateral tubercles or anterior marginal tubercle). This morphology corresponds to the rank 1 of Dobson and Trinkaus (2002). In anterior view, there is a clear incisura submentalis. The anterior surface is slightly concave below the incisors but there is

no *incisura mandibulae anterior*. On the posterior side of the symphyseal region, there is a modest *planum alveolare*. One small foramen is present below the alveolar border on both sides of the symphyseal line, this line being visible along 7mm. The *planum alveolare* is concave under the I_1 and I_2 alveolus edges and is limited inferiorly by the thickening of a prominent superior transverse torus. Below, the fossa genioglossa, although still covered by concretions, is rather deep as shown by the virtual data (Fig.4b), and a foramen geni is visible at its lower limit. The inferior transverse torus is also well developed and both torus can easily be seen on the symphyseal outline (SOM Fig. S6). Inferiorly, the digastric impression form a 19.2 x 9.6 mm large well delineated fossa that is orientated inferior-posteriorly (mostly inferior). This fossa extends laterally up to the level of the P_3.

3.3 Lateral corpus and ramus

The lateral corpus is massive and tall. The alveolar and basilar margins are parallel, so that the height of the corpus is sub-constant from the symphysis to the M_2 level. The bone is thick and shows a strong swelling on the external face of the C, and P_3 sockets. On the external face, a single and large mental foramen (6 mm x 4.6 mm) is present and opens laterally. This foramen is located below the distal part of the first molar and in the inferior vertical half of the mandibular body. Posterior to the foramen, a swelling of the corpus corresponds to a conspicuous *torus lateralis*. Below this torus, the surface is flat and not depressed by an *intertoralis sulcus*. A very thick lateral prominence is also visible at the distal limit of the fragment and was then located below the third molar. Along the basal border, an anterior marginal tubercle is present below the C,/P_3 interalveaolar septum. A very thick, well individualized and projecting posterior marginal tubercle is also present below the mental foramen. These two tubercles are linked by the thickening of a conspicuous marginal torus.

On the lingual side, the mylohyoid line is a rather sharp and straight crest. It crosses the corpus diagonally and the preserved morphology shows its low position below the M_3 alveolar border. The mylohyoid line limits superiorly a very deep submandibular fossa. Above the line, the surface remains flat up to the alveolar border. The superior transverse torus is restricted to the symphyseal region and does not extend laterally. There is a slight thickening of the alveolar border between M_2 and M_3, but there is no real *torus mandibularis*. On the very small part of the ramus that is preserved, we can notice on the lateral side the presence of a crest for the insertion of the masseter muscle that runs supero-anteriorly. On the inner/medial side, the extremity of the mylohyoid groove is present.

In inferior view, the basal border is evenly rounded and its thickness does not decrease posteriorly. The projection of the posterior marginal tubercle is well visible.

3.4 Morphology of the teeth

The state of preservation and heavy attrition of the teeth (Fig. 5) prevent an assessment of the dimensions and the morphology of the crowns. On the M_1, the tiny portion of enamel that is left only shows traces of the groove between the metaconid and entoconid. On the P_4, the portion of enamel that is preserved shows traces of grooves on the disto-buccal part of the crown that suggest the presence of accessory ridge(s) or cusps, but not enough is preserved to assess its morphology. The shape of the crown also appears rather symmetrical but again, the stage of wear prevents from confidently assessing its morphology.

Based on the sediment imprints of the alveolar sockets, all incisors, the canine and the lower right P_3 are single-rooted. While the P_3 root appears to be elliptical in cross-section, the preserved P_4 root is C-shaped with the opening of the "C" facing towards the lingual aspect of the mandible (SOM Fig. S3). The P_3 root has the same length as the canine root (SOM Fig. S7). The M_1 has one mesial and one distal root which are bifurcated at about one third of the

root length below the enamel-cementum junction (cervix). The roots of the M_2 are more robust than those of the M_1 although a full description is impeded by the hole drilled through the centre of the tooth. Medical CT-scan data obtained before the drilling however reveals the presence of a buccal accessory root (SOM Fig. S8). This notwithstanding, the mesial and buccal roots do not appear to be aligned mesio-distally but are rather rotated by about 45 degrees (SOM Fig. S8). The M_2 root is about the same length as that of the canine and P_3 (SOM Figs. S7 and S8).

4. Results of the comparative analyses

4.1 Morphological features of the mandible

As stated above, the Payre 15 symphyseal profile is receding and the anterior aspect of the symphysis does not show any element of a *mentum osseum*. This symphyseal morphology aligns this mandible with the Middle Pleistocene hominins. Upper Pleistocene Neandertals usually have a vertical profile and exhibit some elements of the *mentum osseum*, in particular a *tuber symphyseos* of variable projection (rank 2-3 of Dobson and Trinkaus Table 1). As a result, a rank 1 of the *mentum osseum*, as observed on Payre 15, is found on 80% of the MPH, but only 25% of the EN, 13.6% of the LN and is never observed on EMH (Table 1).

On the lateral body, the posterior location of the mental foramen ($\geq M_1$) and lateral prominence (below M_3) is a derived combination of features of the Neandertal lineage (e.g. Stringer et al., 1984; Trinkaus, 1988; Rosas et al., 1991; Rosas, 2001) that is present on Neandertals at a very high frequency and is already common on the MPH specimens (Table 1). None of the EMH specimens in our comparative sample show a mental foramen posterior to the P_4/M_1 interalveolar septum nor a lateral prominence posterior to the M_2/M_3 septum. By contrast, none of the MPH and Neandertals present a mental foramen anterior to the P_4

alveolus and it is below or posterior to the P_4 alveolus on more than 90% of these samples. Similarly, a lateral prominence below the M_2 alveolus is never observed on MPH and EN, and is recorded in only 6.7% of the LN sample (Table 1). For both these features, Payre 15 aligns clearly with the Neandertal lineage. As regards the number of foramina, the presence of one single mental foramen, such as on Payre 15, is the pattern observed on the vast majority of EMH (92.6%) and two third of the MPH whereas more than half of the Neandertals present multiple foramina. Finally, on Payre 15, the mylohyoid line follows a diagonal orientation as it is observed on 92% of the Neandertals, 68% of the MPH and 44% of the EMH. The mylohyoid line is at a low position below the M_3, a pattern observed on 92% of the MPH, one third of the EN and only 12% and 4% of the LN and EMH respectively.

It is noteworthy that the combination observed on Payre 15 for the state of six morphological features (*mentum osseum* development, number and location of the mental foramen, location of the lateral prominence and pattern of the mylohyoid line) is only observed on MPH (44.4%, n = 9), but never on both EMH and Neandertals. However, among MPH, this combination of features is present only on individuals from Sima de los Huesos. Excluding the mylohyoid line position and orientation, the combination of a mentum osseum rank 1 with a posterior location of the mental foramen and lateral prominence that is scored on Payre 15 can be found on Neandertals (17%) but is still much more common on MPH (56%). Finally, the other two Neandertals that are usually attributed to the MIS 7, Ehringsdorf F and Montmaurin, differ from Payre 15 by a slightly more developed *mentum osseum* (rank 2, contra Vialet et al., 2018) and a non-oblique mylohyoid line. Payre 15 is however morphologically closer to Ehringsdorf F than to Montmaurin, due to the more anterior location of the mental foramen and lateral prominence on the latter.

4.2 Mandibular dimensions

Overall, Neandertals and EMH differ little in terms of mandibular body height and breadth. Compared to these samples, Payre 15 is overall large with a tall body (Table 2). The estimated bi-M_2 width of the mandible falls above the mean of all comparative groups. It belongs to the upper half of their range of variation, being closer to Late Neandertals (Azs = 0.06) than to EN or MPH (Table 2). On the bivariate plot of the bi-M_2 width against the height of the body at M_1 (Fig. 6), the groups overlap entirely but Payre 15 falls among the tallest and rather wide specimens.

For the dimensions of the body at the symphyseal region, Payre 15 falls well within the variation of all the comparative samples. Its height (HS: 35.7 mm) is above the mean of all groups, being closer to the EN. Its thickness (ES: 16.2) is high, falling in the upper half of the range of all comparative groups and above their means (which are in addition very close to each other). The resultant robusticity index (INDS) is slightly above the mean of the EN and LN, very close to the MPH mean and slightly below the EMH average.

Posteriorly, the mandibular body of Payre 15 remains tall, with heights falling well above the means of all comparative groups and in the upper half of their ranges of variation. At M_1, its height is among the highest values of our comparative samples, being exceeded by only two specimens from Sima de los Huesos and the Aterian El Harhoura mandible. The lateral body is in addition thick in absolute values (Table 2). At the level of the M_1 and M_2, the thickness is close to the MPH mean but well above the means and in the upper halves of variation of NEAN and EMH. At P_4, the thickness of Payre 15 is outside the EMH range of variation (Azs = 1.09). When chronological subgroups of Neandertals are considered separately, the thickness of Payre 15 at P_4 is also excluded from the variation of Late Neandertals. When compared to MPH, the thickness of Payre along the premolars and molars falls well within the Sima de los Huesos variation, above the thickness of Arago 2, close to

Mauer and well below the Arago 13 individual.

Although the mandible is quite thick anteriorly when assessed relatively to its height, at the level of the postcanine teeth, the mandible is not particularly thick given its height. The robusticity index at P_4 is above the means of EMH and LN, but below the EN mean and well below the Arago 2, Arago 13 and Mauer indices. At M_1 and M_2, the robusticity indices fall below the mean and in the lower half of variation of MPH and Neandertals (Azs between -0.1 and -0.4), but slightly above the EMH mean (Table 2).

Overall, when compared to the MPH, one can notice that the dimensions of the Payre 15 mandibular corpus are within the range of variation of the Sima de los Huesos sample. Its heights and breadths are above those of Arago 2, close or above Mauer and well below Arago 13. The robusticity indices are also within the Sima de los Huesos range but below the indices of all the other MPH specimens. Payre 15 is also wider, thicker but mostly taller than Ehringsdorf F and Montmaurin, so that the robusticity indices are also lower than on these two supposedly MIS 7 specimens.

4.3 Principal Component Analyses of the mandibular dimensions

The first multivariate analysis, a PCA of the raw values for five variables (height and breadth at the symphysis and at the M_1, bi-M_2 width) is dominated by a clear size effect along PC1 and the relative thickness and width of the mandibular corpus (Fig. 7a).

The scatterplot of individuals on PC1 vs. PC2, which accounts for more than 79 % of the total variation, tends to separate EMH from NEAN and MPH along PC2 (which is strongly correlated negatively with bi-M_2 width) and indicates large individual variation within the three groups along PC1. According to its score along PC1, Payre 15 is among the largest mandibles analysed here, confirming the results of uni- and bi-variate analyses; and its position in the lower-right quadrant of the graph points to its wide and robust mandibular

corpus, with large thickness relative to height at the symphysis and large height of the corpus at M_1.

The second multivariate analysis (Fig. 7b), a between group PCA of the LSRs for the same five variables, distinguishes mainly EMH from Neandertals and MPH, although there is a partial overlap between those groups, mainly because of the *H. sapiens* mandible from Pataud which exhibits a particularly large thickness of its corpus at M_1. There is also substantial overlap between MPH and Neandertals with this combination of variables. The correlations of variables with the bgPCs as well as the position and orientation of the convex hulls for MPH and Neandertals indicate that their mandibles mainly differ in the relative size of their corpus at the two levels measured here. MPH mandibles tend to show a large (i.e. thick and high) corpus at the M_1 and a relatively small symphysis region, while the opposite trend is observed in Neandertals (and EMH) mandibles, which present a relatively larger symphysis. Payre 15 has positive values for bgPC2 and around zero for bgPC1, which corresponds mainly to the large dimensions of its posterior corpus (height and thickness of the corpus at M_1). Payre shows greater morphometric affinities with MPH individuals Mauer and AT-605, as well as the Neandertal Shanidar 1 which is its closest neighbour in this analysis.

4.4 Elliptic Fourier Analysis of the symphyseal profile

We present here the results obtained for the first two Principal Components (PC), which account for more than 80% of the total variation (Fig. 8). Positive values for PC1 (71.3 % of total variance) correspond to thin symphysis with a marked *mentum osseum* (well defined *incurvatio mandibulae anterior* and *tuber symphyseos*), while for negative values, the profile is thicker. The variation along PC2 (12.7 % of total variance) shows for positive values

a rather thin symphysis with a vertical anterior profile, and for negative values, a symphysis that is slightly receding anteriorly and thick anteroposteriorly, with marked reliefs (planum alveolare, fossa genioglossa, superior and inferior transverse torus). On the PC1/PC2 plot, the distribution of the MPH is well separated from the other groups. The distributions of EMH and Neandertals overlap. However the latter show more negative values on PC1 because of their rather thick and vertical symphyseal profile. The MPH sample presents a morphology similar than the Neanderthal one along PC1 while, on PC2 their values are more negative, due to the important thickness of the profile. On this plot, Payre 15 falls just outside the Neandertal variability, among the lowest values on PC2 and close to the Mauer and Sima de los Huesos AT-1 mandibles. Interestingly, Montmaurin also falls among the lowest values on PC2 and in the MPH range.

4.5 First molar root metrics

The PCA of the four root metrics reveals that root length (RL) and cervical plane area (CPA) account for the variation along PC1, while variations in the volumes of the root portions (cervical and apical: Vcv and Vap) are found along PC2 (Fig. 9a). The RMH M_1 roots (negative PC1 values only) are generally smaller than those of the EMH and NEAN samples. Payre 15 is within the non-overlapping NEAN range, i.e. it has long roots and a large cervical base similar to the MPH specimen from Mauer (PC1). In terms of the root volumetric proportions (PC2) Payre 15 is just outside the EMH cluster and well within the Neandertal range. The volumetric bifurcation index of the Payre 15 M_1 root is 54.34% which classifies this specimen as mesotaurodont. When regressed against cervical plane area as a proxy for occlusal area, the M_1 root of Payre 15 falls above the reduced major axis regression line, i.e. it has relative large root surface area for its cervical plane area (Fig. 9b). The Payre 15 M_1 root surface area is well outside the RMH range but it falls within the upper end of the

NEAN variation and is somewhat smaller than that of MPH and several EMH individuals (Fig. 9c).

5. Discussion and conclusions

The Payre 15 mandible adds one very important specimen to the Middle Pleistocene hominin sample found at the site. It was recovered in the same layer (Ga) and spatially close to five isolated teeth and a parietal fragment previously identified (SOM Fig. S1 and Condemi and Moncel, 2008). The heavy occlusal wear of the Payre 15 lower P_4 and M_1 suggests that it belonged to a rather old adult individual. Despite this heavy wear and some slight alveolar resorption, the individual was likely still able to masticate. Four of the isolated teeth previously found in the same layer, a lower canine, and three lower premolars show little occlusal attrition and therefore do not belong to the same individual as Payre 15. However, one tooth, the isolated Payre 12 upper left molar (most likely a M_2 according to Condemi and Moncel, 2008) that was found in 1999 is heavily worn. It also shows a strong asymmetry of its occlusal surface, the buccal cusps being much more worn than the lingual ones, following a wear pattern congruent with what is observed on Payre 15. We however could not get access to this specimen to test its possible attribution to the same individual as Payre 15. Interestingly, the four other teeth from level Ga, as well as the teeth found in levels D, E, F and Gb, all belong to younger individuals who were children, adolescent or young adults (Condemi and Moncel, 2008). Finally, it is noteworthy that the morphology of the breakage and notches on the mandibular ramus indicate that this individual may have been consumed by a carnivore.

Besides the site of Payre, the discovery of this mandible adds a valuable specimen to the European hominin fossil record, which is particularly scarce for the MIS 8-6 period. The

two mandibles from Ehringsdorf F (Mallick and Frank, 2002; Schüler, 2003) and Montmaurin are attributed to the MIS 7, but precise chronological data for Montmaurin are lacking (Vialet et al., 2018). This is also the case for the Aubesier 11 mandible that might date to MIS7/6 but lacks a more precise chronological attribution (Lebel et al., 2001).

Overall, our analyses show that when compared to *H. sapiens* and Upper Pleistocene Neandertals, Payre 15 exhibits a primitive symphyseal outline and anterior symphysis, associated with a tall lateral corpus showing a Neandertal-derived morphology. In terms of size, the Payre 15 mandibular corpus is rather thick but mostly tall. Its height values at M_1 and M_2 exceed those of all the MIS 5d-3 Late Neandertals included in our samples, and fall among or above the highest values of Early Neandertals and MIS 12-9 European hominins. In contrast to it's relatively thick symphysis, Payre 15 has a relatively narrow lateral corpus at the level of the molars when assessed relative to its height. Payre 15 has mesotaurodont M_1 roots as are common in both MPH (Mauer and Mala Balanica) and Neandertals but not in EMH (Kupczik and Hublin, 2010; Skinner et al., 2016; Kupczik et al., 2019). The M_1 roots of Payre 15 are relatively long and have a large root surface area (absolute and when scaled against cervical plane area) and fall within the upper size range of Neandertals. The root size is close to the median of EMH roots but smaller than those of MPH roots (Fig. 9). The presence of an accessory buccal root in the M_2 of Payre 15 (Fig. 4; SOM Fig. S8) is noteworthy given that three-rooted mandibular molars are rare in non-Asian *H. sapiens* but occur with high frequency among modern Asian populations and the Denisovan hemimandible from Xiahe (China), suggesting gene flow between the two (Bailey et al., 2019; Chen et al., 2019). Yet, while the third accessory roots of the archaic and modern Asian populations are present on either the distolingual aspect or lingually between the mesial and distal roots (Bailey et al., 2019), in Payre 15 the accessory root is positioned on the buccal aspect of the M_2 (Fig. 4; SOM Fig. S8). Whether or not the presence of three-rooted

mandibular molars between these Middle Pleistocene European and Asian hominins are the result of possible admixture between the two requires further research.

As regards its morphology, Payre 15 is characterized by a receding symphyseal profile without any element of the mentum osseum, associated with a posteriorly and inferiorly located single mental foramen and a posterior location of the lateral prominence (the last two features being highly correlated, Rosas, 2001). The lateral corpus displays moderate to well-developed structures on its external and inner sides (anterior marginal tubercle, prominent posterior marginal tubercle and lateral prominence, intertoralis sulcus, prominent mylohyoid line and deep submandibular fossa).

The posterior location of both the mental foramen and lateral prominence clearly aligns this mandible with the Neandertals (e.g. Trinkaus, 1988; Rosas, 2001; Nicholson and Harvati, 2006). These features are already present on MPH at a very high frequency. The presence of a deep submandibular fossa is also a shared feature with Neandertals that can be found on MPH, although at lower frequencies (Rosas, 2001; Mounier et al., 2009). By contrast, the morphology of its anterior symphysis distinguishes Payre 15 from the vast majority of the MIS 6-3 Neandertals, and aligns it better with the MIS 11-9 MPH sample. This is also shown by the results of the Elliptic Fourier analysis of the symphyseal outline, with Payre 15 falling very close to the Mauer and Sima de los Huesos AT1 specimens. The low position of its mylohyoid line is a primitive feature (e.g. Rosas and Bermúdez de Castro, 1999) that is almost constant on MPH but more rarely retained by Neandertals (being even less frequent on Late than Early Neandertals) and EMH. Similarly, the thickness of the basal border remains constant from the symphysis to the level of the M_3 (near the gonion), another feature that is shared with MPH whereas it usually decreases posteriorly in Neandertals (Rosas, 2001). The large and deep incisura submentalis is also a feature that brings Payre 15 closer to pre-MIS 6 MPH than to MIS 5-3 Neandertals (Mounier et al., 2009), although this

feature is quite variable in all samples. Interestingly, Payre 15 shows several derived Neandertal features on its external side, whereas the inner side of the body is less derived, which adds to previous evidence suggesting that morphological changes leading to the full Neandertal mandibular derived morphology were expressed earlier on the external side of the corpus than on its inner side (Rosas, 2001).

Despite the "primitive" shape of its symphysis, Payre 15 lacks an extended planum alveolare that is seen on all MIS 7-11 European Middle Pleistocene hominins (Mounier et. al., 2009), including Montmaurin and Ehringsdorf F. The mylohyoid line, with a low position at the level of the M_3 but diagonally crossing the corpus, presents an "intermediate" position between the low and parallel pattern seen in Lower and Middle Pleistocene *Homo* specimens and the high and oblique position of most Upper Pleistocene Neandertals (Rosas, 2001). This pattern is similar to what has been observed on most of the Sima de los Huesos sample (Rosas, 2001).

Payre 15 differs from the majority of MIS 6-5e Early Neandertals by the more archaic morphology of its symphysis and inner corpus. Compared to MIS 7 Neandertals, Payre 15 is both morphologically and metrically closer to Ehringsdorf F than to Montmaurin. It shares with Ehringsdorf F and Aubesier 11 the posterior location of the lateral prominence and mental foramen, whereas these structures are more anterior on the Montmaurin mandible, which also differs in presenting multiple foramina. In addition, Ehringsdorf F and Montmaurin differ from Payre 15 by the presence of an incipient tuber symphyseos. Rosas (1997) and Rosas and Bastir (2004) have detected an allometric effect in several morphological traits on the lateral body and in the symphyseal outline and orientation among the Sima de los Huesos sample. That, in relation with sexual dimorphism, may explain part of this variation, and in particular as regards the lack of retromolar space on Montmaurin (see also Nicholson and Harvati, 2006). It is noteworthy, however, that a posterior location of the

mental foramen and lateral prominence is observed on tall and large specimens such as Payre 15 and Ehringsdorf F but also on the smaller Aubesier 11 mandible.

By its dimensions and combination of features, Payre 15 falls well within the variation of Middle Pleistocene European hominins and is distinct from Upper Pleistocene Neandertals by a number of features. Although its morphology aligns it clearly with the Neandertal lineage, its combination of metric and morphological features is unique among post MIS 9 specimens (Table 1). This combination recalls some specimens of the much older MIS 11 site of Sima de los Huesos, which might suggest, despite the limitations due to the very small sample size for this time period, that little morphological change occurred on the Neandertal mandibular symphysis and corpus during these 200 000 years.

If Payre 15, Montmaurin, Ehringsdorf F and Aubesier 11 are of close chronological ages, they all document the persistence of a plesiomorphic morphology at the mandibular symphysis (rank 1-2 of Dobson and Trinkaus, 2000) and to a lesser extent on the inner side of the body, but they also document some degree of morphological variation. This apparent low level of diachronic changes and rather high synchronic variability may be seen as an argument to reject the accretion model, and one in favor of a two-phases or multiple hominin taxa model as suggested by some authors (Rosas et al., 2006; Arsuaga et al., 2014; Bermudez de Castro et al., 2018; Vialet et al., 2018; but see Rosas et al., 2019 for a contradictory viewpoint). However, the accretion model postulates a mosaic pattern of variation and changes as well as a trend toward a reduction in the variability through time to which the observed data - in our view - are not incompatible, given the chronological ages of these specimens.

Certainly the difficulty in testing these models lies in the scarcity of the hominin fossil record for the chronological period between the MIS 9 and 5, which prevents a statistical assessment of morphological variation through time and space. The high number of hominin

remains found at Sima de los Huesos, which represent a subpopulation of closely related individuals (Arsuaga et al., 2014) creates a sample bias within the mid- Middle Pleistocene hominin fossil record that necessarily affects our ability to interpret the observed morphological variability at a larger scale. Such a bias also certainly affects our ability to test the various scenarios proposed to explain the history of the peopling of Europe in the Middle Pleistocene and the driving forces underlying the origins and evolutionary history of the Neandertal lineage. By adding a new hominin specimen to the poor MIS 7 fossil record, the Payre 15 mandible brings new evidence to better characterize the morphological variability of the hominins who occupied Europe in the Middle Pleistocene and to investigate whether these hominins represent different demes within a single polymorphic species or different taxa.

Acknowledgements

For access to comparative specimens we thank the following institutions and individuals: Thüringisches Landesamt für Denkmalpflege und Archäologie Weimar (T. Schüler); Musée d'Archéologie nationale (C. Schwab); Musée d'Angoulême (J.-F.Tournepiche); Fondation Institut de Paléontologie Humaine (H. de Lumley); Musée d'Art et d'Archéologie du Périgord (V. Merlin-Langlade); Croatian National History Museum and the Croatian Academy of Science and Arts (J. Radovčić, D. Brajkovič); Moravian Museum (P. Neruda); Geologisch-Paläontologisches Institut der Universität Heidelberg (U. A. Glasmacher); Iziko South African Museum (W. Black); (Royal Belgian Institute of Natural Sicences (P. Semal); A. Rosas (CSCIC, Museo Nacional de Ciencias Naturales, Madrid) ; M. Toussaint (Service archéologique de Wallonie); B. Vandermeersch (Université de Bordeaux). We also would like to thank Adeline Le Cabec for her attempt to improve our segmentation of the mandible. This research was supported by the Max Planck Society (Germany) and the Centre National de la

Recherche Scientifique (France). We are grateful to Camille Daujeard (CNRS, UMR 7194, Paris, France) for her help and feedback regarding the taphonomic description of the mandible and the interpretation of the observed marks. Fieldwork at Payre was financially supported by the French Ministry of Culture (Rhône-Alpes region) and the regional area (Département de l'Ardèche).

References

Adams, D. C., Collyer, M. L. , Kaliontzopoulou, A., Sherratt, E., 2017. Geomorph: Software for geometric morphometric analyses. R package version 3.0.5. https://cran.r-project.org/package=geomorph**.**

Arnaud, J., Peretto, C., Grimaud-Hervé, D., 2015. The Grotta Guattari mandibular remains in the Italian human evolutionary context: A morphological and morphometrical overlook of the Neanderthal jaw. Quaternary International 388, 206–217.

Arsuaga, J. L., Martínez, I., Gracai, A., Lorenzo, C., 1997. The Sima de los Huesos crania (Sierra de Atapuerca, Spain). A comparative study. Journal of Human Evolution 33, 219-281.

Arsuaga, J.L., Martínez, I., Arnold, L. J., Aranburu, A., Gracia-Téllez, A., Sharp, W. D., Quam, R. M., Falguères, C., Pantoja-Pérez, A., Bischoff, J., Poza-Rey, E., Parés, J. M., Carretero, J. M., Demuro, M., Lorenzo, C., Sala, N., Martinón-Torres, M., García, N., Alcázar de Velasco, A., Cuenca-Bescós, G., Gómez-Olivencia, A., Moreno, D., Pablos, A., Shen, C.-C., Rodríguez, L., Ortega, A. I., García, R., Bonmatí, A., Bermúdez de Castro , J. M., Carbonell, E. , 2014. Neandertal roots: Cranial and chronological evidence from Sima de los Huesos. Science 344, 1358-1363.

Baena, J., Moncel, M-H., Cuartero, F., Chacón, M. G., Rubio, D., 2017. Late Middle Pleistocene genesis of Neanderthal technology in Western Europe. The case of Payre site (south-east France). Quaternary International 436, 212-238.

Bailey, S. E., Hublin, J.-J., Antón, S.C., 2019. Rare dental trait provides morphological evidence of archaic introgression in Asian fossil record. Proceedings of the National Academy of Sciences 116, 14806-14807.

Bermúdez de Castro, J.M., Martinón-Torres, M., Rosell, J., Blasco, R., Arsuaga, J.L., Carbonell, E., 2016. Continuity versus discontinuity of the human settlement of Europe between the late Early Pleistocene and the early Middle Pleistocene. The mandibular evidence. Quaternary Science Reviews 153, 51-62.

Bermúdez de Castro, J.M., Martinón-Torres, M., Martínez de Pinillos, M.M., García-Campos, C., Modesto-Mata, M., Martín-Francés, L., Arsuaga, J.L., 2018. Metric and morphological comparison between the Arago (France) and Atapuerca-Sima de los Huesos (Spain) dental samples, and the origin of Neanderthals. Quaternary Science Reviews, https://doi.org/10.1016/j.quascirev.2018.04.003

Bocherens, H., Díaz-Zorita Bonilla, M., Daujeard, C., Fernandes, P., Raynal, J-P., Moncel, M-H., 2016. Direct isotopic evidence for subsistence variability in Middle Pleistocene Neanderthals (Payre, France), Quaternary Science Review 154, 226-236.

Bonhomme, V., Picq, S., Gaucherel, C., Claude, J., 2014. Momocs: Outline Analysis Using R. Journal of Statistical Software 56, 1-24.

Carmignani, L., Moncel, M-H., Fernandes, P., Wilson, L., 2017. Technological variability during the Early Middle Palaeolithic in Western Europe. Reduction systems and predetermined products at the Bau de l'Aubesier and Payre (South-East France). PLoS ONE 12, e0178550.

Chacón Navarro, M. G., Détroit, F., Coudenneau, A., Moncel, M-H. 2016. Morphometric assessment of convergent tool technology and function during the Early Middle Palaeolithic: the case of Payre, France. PLoS ONE 11, 0155316.

Chen, F., Welker, F., Shen, C.-C., Bailey, S.E., Bergmann, I., Davis, S., Xia, H., Wang, H., Fischer, R., Freidline, S.E., Yu, T.-L., Skinner, M.M., Stelzer, S., Dong, G., Fu, Q., Dong, G., Wang, J., Zhang, D., Hublin, J.-J., 2019. A late Middle Pleistocene Denisovan mandible from the Tibetan Plateau. Nature 569, 409-412.

Claude, J., 2008. Morphometrics with R., Springer, New York.

Condemi, S., Moncel, M.-H., 2008. Les restes humains, in: Moncel, M.-H. (Ed), Le Site de Payre. Occupations humaines dans la Vallée du Rhône à la Fin du Pléistocène Moyen et au Début du Pléistocène Supérieur, Mémoire de la Société Préhistorique Française, XLVI, Paris, pp. 131-151.

Corny, J., Détroit, F., 2014. Anatomic identification of isolated modern human molars: Testing procrustes aligned outlines as a standardization procedure for elliptic fourier analysis. American Journal of Physical Anthropology 153, 314–322.

Darroch, J.N., Mosimann, J.E., 1985. Canonical and principal components of shape. Biometrika 72, 241–252.

Daujeard, C., Moncel, M.-H., 2010. On Neanderthal subsistence strategies and land use: A regional focus on the Rhone Valley area in southeastern France. Journal of Anthropological Archaeology 29, 369-391.

Daujeard, C., Moncel, M.-H., Rivals, F., Fernandez, P., Auguste, P., Aureli, D., Bocherens, H., Crégut-Bonnoure, E. Debard, E., Liouville, M., 2011. Quel type d'occupation dans l'ensemble F de Payre (Ardèche, France) ? Halte de chasse spécialisée ou campement de courte durée ? Un exemple d'approche multi-disciplinaire, in: Costamagno, S., Bon, F., Valdeyron N. (Eds), Les Haltes de Chasse en Préhistoire : Quelles Réalités Archéologiques ?, Palethnologie 3, Toulouse, pp. 77-103.

Daura, J., Sanz, M., Arsuaga J.L., Hofffmann, D.L., Quam, R.M., Ortega, M. C., Santos, E., Gómez, S., Rubio, A., Villaescusa, L., Souto, P., Mauricio, J., Rodrigues, F., Ferreira, A.,

Godinho, P., Trinkaus, E., Zilhão, J., 2017. New Middle Pleistocene hominin cranium from Gruta da Aroeira (Portugal)." Proceedings of the National Academy of Sciences 114, 3397-3402.

Dean, D., Hublin, J.J., Hollowy, R., Ziegler, R., 1998. On the Phylogenetic position of the pre-Neandertal specimen from Reilingen, Germany. Journal of Human Evolution 34**,** 485-508.

Dennell, R.W., Martinón-Torres, M., Bermúdez de Castro, J.M., 2011. Hominin variability, climatic instability and population demography in Middle Pleistocene Europe, Quaternary Science Reviews 30, 1511-1524.

Dobson, S.D., Trinkaus, E., 2002. Cross-sectional geometry and morphology of the mandibular symphysis in Middle and Late Pleistocene *Homo*. Journal of Human Evolution 43, 67-87.

Ecker, M., Bocherens, H., Julien, M-A., Rivals, F., Raynal, J-P., Moncel, M-H., 2013. Middle Pleistocene ecology and Neanderthal subsistence: Insights from stable isotope analyses in Payre (Ardèche, Southeastern France). Journal of Human Evolution 65, 363-373.

Endicott, P., Ho, S.Y.W., Stringer, C., 2010. Using genetic evidence to evaluate four palaeoanthropological hypotheses for the timing of Neanderthal and modern human origins. Journal of Human Evolution 59, 87-95.

Gómez-Robles, A., 2019. Dental evolutionary rates and its implications for the Neanderthal–modern human divergence. Science Advances 5, eaaw1268.

Gómez-Robles, A., Bermúdez de Castro, J.M., Arsuaga, J.L., Carbonell, E., Polly, D., 2013. No known hominin species matches the expected dental morphology of the last common ancestor of Neanderthals and modern humans. Proceedings of the National Academy of Sciences of the USA 110, 18196-18201.

Grün, R., Aubert, M., Joannes-Boyau, R., Moncel, M.-H., 2008. High resolution analysis of uranium and thorium concentration as well as U-series isotope distributions in a Neanderthal tooth from Payre (Ardèche, France) using laser ablation ICP-MS. Geochimica et Cosmochimica Acta 72, 5278-5290.

Hanegraef, H., Martinón-Torres, M., Martínez de Pinillos, M.M., Martín-Francés, L., Vialet, A., Arsuaga, J.-L., Bermúdez de Castro, J.M., 2018. Dentine morphology of Atapuerca-Sima de los huesos lower molars: Evolutionary implications through three-dimensional geometric morphometric analysis. American journal of Physical Anthropology 166, 276-295.

Hardy, B.L., Moncel, M.-H., 2011. Neanderthal use of fish, mammals, birds, starchy plants and wood 125-250,000 years ago. PLoS ONE 6, e23768.

Harvati, K., Hublin, J.-J., Gunz, P., 2010. Evolution of middle-late Pleistocene human cranio-facial form: A 3-D approach. Journal of Human Evolution 59, 445-464.

Hublin, J. J., 1998. Climatic changes, paleogeography, and the evolution of the Neandertals, in: Akazawa, T., Aoki, K., Bar-Yosef, O. (Eds), Neandertals and Modern Humans in Western Asia. Plenum Press, New York, pp. 295-310.

Hublin, J.-J., 2009. The origin of Neandertals. Proceedings of the National Academy of Sciences of the USA 106, 16022-16027.

Jungers, W.L., Falsetti, A.B., Wall, C.E., 1995. Shape, relative size, and size-adjustments in morphometrics. American Journal of Physical Anthropology 38, 137–161.

Kuhl, FP, Giardina, CR., 1982. Elliptic Fourier features of a closed contour. Computer Graphics and Image Processing 18, 236-258.

Kupczik, K., Hublin, J.-J., 2010. Mandibular molar root morphology in Neandertals and Late Pleistocene and recent *Homo sapiens*. Journal of Human Evolution 59, 525-541.

Kupczik, K., Delezene, L.K., Skinner, M.M., 2019. Mandibular molar root and pulp cavity morphology in *Homo naledi* and other Plio-Pleistocene hominins. Journal of Human Evolution 130, 83-95.

Lebel, S., Trinkaus, E., Faure, M., Fernandez, P., Guérin, C., Richter, D., Mercier, N., Valladas, H., Wagner, G.A., 2001. Comparative morphology and paleobiology of Middle Pleistocene human remains from the Bau de l'Aubesier, Vaucluse, France. Proceedings of the National Academy of Sciences of the USA 98, 11097-11102.

Lestrel, P.E., 1989. Method for analysing complex two-dimensional forms: Elliptical fourier functions. American Journal of Human Biology 1, 149–164.

Lestrel, P.E., 1997. Fourier Descriptors and Their Applications in Biology, Cambridge University Press, Cambridge.

Lili, M., Tianmin, X., Jiuxiang, L., 2009. Validation of a three-dimensional facial scanning system based on structured light techniques. Computer Methods and Programs in Biomedecine 94, 290–298.

Mallick, R., Frank, N., 2002. A new technique for precise uranium-series dating of travertine micro-samples. Geochimica et Cosmochimica Acta 66, 4261– 4272.

Manzi, G., 2016. Humans of the Middle Pleistocene: The controversial calvarium from Ceprano (Italy) and its significance for the origin and variability of *Homo heidelbergensis*. Quaternary International 411, 254-261.

Martin, R., Saller, K., 1957. Lehrbuch der Anthropologie. In Systematischer Darstellung mit Besonderer Berücksichtigung der Anthropologishen Methoden, Gustav Fisher Verlag, Stuttgart.

Martinón-Torres, M., Bermúdez de Castro, J.M., Gómez-Robles, A., Prado-Simón, L., Arsuaga, JL., 2012. Morphological description and comparison of the dental remains from Atapuerca-Sima de los Huesos site (Spain). Journal of Human Evolution 62, 7-58.

Meyer, M., Arsuaga, J.L., de Filippo, C., Nagel, S., Aximu-Petri, A., Nickel, B., Martínez, I., Gracia, A., Bermúdez de Castro, J.M., Carbonell, E., Viola, B., Kelso, J., Prüfer, K., Pääbo, S., 2016. Nuclear DNA sequences from the Middle Pleistocene Sima de los Huesos hominins. Nature 531, 504-507.

Molnar, S., 1971, Human tooth wear, tooth function and cultural variability. American Journal of Physical Anthropology 34, 175-190.

Moncel, M.-H. (Ed), 2008. Le site de Payre. Occupations humaines dans la vallée du Rhône à la fin du Pléistocène moyen et au début du Pléistocène supérieur, Mémoire de la Société Préhistorique Française, XLVI, Paris.

Moncel, M.H., Chacón, M.G., Coudenneau, A., Fernandes, P., 2009. Points and convergent tools in the European Early Middle Palaeolithic site of Payre (SE, France). Journal of Archaeological Science 36, 1892-1909.

Moncel, M.-H., Condemi, S., 2007. The human remains of the site of Payre (S-E France, OIS 7-5): Remarks on Stratigraphic position and interest. Anthropologie Brno XLV/1, 7-17.

Moncel, M.-H., Daujeard, C., 2012.The variability of the Middle Palaeolithic on the right bank of the Middle Rhône Valley (southeast France): Technical traditions or functional choices? Quaternary International 247, 103-124.

Moncel, M-H, Fernandes, P., Willmes, M., James, H., Grün, R., 2019. Rocks, teeth, and tools: New insights into early Neanderthal subsistence strategies in South-Eastern France from lithic reconstructions and strontium isotope analysis. PLoS One 14, e0214925.

Mounier, A., Marchal, F., Condemi, S., 2009. Is *Homo heidelbergensis* a distinct species? New insight on the Mauer mandible. Journal of Human Evolution 56, 219–246.

Nicholson, E., Harvati, K., 2006. Quantitative analysis of human mandibular shape using three-dimensional geometric morphometrics. American Journal of Physical Anthropology 131, 368-383.

Osborn, J.W., 1982. Helicoidal plane of dental occlusion. American Journal of Physical Anthropology 57, 273-281.

Prüfer, K., Racimo, F., Patterson, N., Jay, F., Sankararaman, S., Sawyer, S., Heinze, A., Renaud, G., H. Sudmant, P.H., de Filippo, C., Li, H., Mallick, S., Dannemann, M., Fu, Q., Kircher, M., Kuhlwilm,M., Lachmann, M., Meyer, M., Ongyerth, M., Siebauer, M., Theunert, C., Tandon, A., Moorjani, P., Pickrell, J., Mullikin, J.C., Vohr, S.H., E. Green, R.E., Hellmann, I., Johnson, P.L.F., Blanche, H., Cann, H., Kitzman, J.O., Shendure, J., Eichler, Lein, E.E., Bakken, T.E., Golovanova, L.V., Doronichev, V.B., Shunkov, M.V., Derevianko, A.P., Viola, B., Slatkin, M., Reich, D., Kelso, J., Svante Pääbo, 2014. The complete genome sequence of a Neandertal from the Altai Mountains. Nature 505, 43-49.

R Core Team, 2017. R: A language and environment for statistical computing, R Foundation for Statistical Computing, Vienna, Austria.

Rivals, F., Moncel, M.-H., Patou- Mathis, M., 2009. Seasonality and intra-site variation of Neanderthal occupations in the Middle Palaeolithic locality of Payre (Ardèche, France) using dental wear analyses. Journal of Archaeological Science 36, 1070-1078.

Roksandic, M., Mihailović, D., Mercier, N., Dimitrijević, V., Morley, M.W., Rakočcević, Z., Mihailović, B., Guibert, P., Babb, J., 2011. A human mandible (BH-1) from the Pleistocene deposits of Mala Balanica cave (Sićevo Gorge, Niš, Serbia). Journal of Human Evolution 61, 186-196.

Roksandic, M., Predrag Radović, P., Joshua Lindal, J., 2018. Revising the hypodigm of *Homo heidelbergensis*: A view from the Eastern Mediterranean. Quaternary International 466, 66-81.

Rosas, A., 1997. A gradient of size and shape for the Atapuerca sample and middle Pleistocene hominid variability. Journal of Human Evolution 33, 319-331.

Rosas, A., 2001. Occurrence of Neanderthal features in mandibles from the Atapuerca-SH site. American Journal of Physical Anthropology 114, 74-91.

Rosas, A., Bastir M., 2004. Geometric morphometric analysis of allometric variation in the mandibular morphology of the hominids of Atapuerca, Sima de los Huesos Site. The Anatomical Record, Part A 278A, 551-560.

Rosas, A., Bastir, M., Alarcón, J.A., 2019. Tempo and mode in the Neandertal evolutionary lineage: A structuralist approach to mandible variation. Quaternary Science Reviews, 62-75.

Rosas, A., Bastir, M., Martínez Maza, C., Bermúdez de Castro, J.M., 2002. Sexual dimorphism in the Atapuerca-SH hominids. The evidence from the mandibles. Journal of Human Evolution 42, 451–474.

Rosas, A., Bastir, M., Martínez-Maza, C., García-Tabernero, A., Lalueza-Fox, C., 2006. Inquiries into Neanderthal craniofacial development and evolution: "accretion" versus "organismic" models, in: Harvati, K., Harrison, T. (Eds). Neanderthals Revisited: New Approaches and Perspectives, Springer, New York, pp. 37–70.

Rosas, A., Bermúdez de Castro, J.M., 1997. The Mauer Mandible and the evolutionary significance of *Homo heidelbergensis*. Geobios 31, 687-697.

Rosas, A., Bermúdez de Castro, J.M., 1999. The ATD6-5 mandibular specimen from Gran Dolina (Atapuerca, Spain). Morphological study and phylogenetic implications. Journal of Human Evolution 37, 567-590.

Rosas A., Bermúdez de Castro, J.M., Aguirre, E., 1991. Mandibules et dents d'Ibeas (Espagne) dans le contexte de l'Evolution humaine en Europe. L'Anthropologie 95, 89-102.

Schüler, T., 2003. ESR dating of a new Paleolithic find layer of the travertine site of Weimar-Ehringsdorf (Central Germany). Terra Nostra 2, 233-235

Scolan, H., Santos, F., Tillier, M.-A., Maureille, B., Quintard, A., 2012. Des nouveaux vestiges néanderthaliens à Las Pélénos (Monsempron-Libos, Lot-et-Garonne, France). Bulletins et Mémoires de la Société d'Anthropologie de Paris 24, 69-95.

Singleton, M., 2002. Patterns of cranial shape variation in the Papionini (Primates: Cercopithecinae). Journal of Human Evolution 42, 547–578.

Skinner, M. M., De Vries, D., Gunz, P., Kupczik, K., Klassen, R.P., Hublin, J.-J., Roksandic, M., 2016. A dental perspective on the taxonomic affinity of the Balanica mandible (BH-1). Journal of human evolution 93, 63-81.

Stringer, C., 2012. The status of *Homo heidelbergensis* (Schoetensack 1908). Evolutionary Anthropology 21, 101-107.

Stringer, C.B., Hublin, J.-J., Vandermeercsh, B., 1984. The origin of anatomically modern humans in Western Europe, in: Smith, F.H., Spencer, F. (Eds), The Origins of Modern Humans, a World Survey of Fossil Evidence, Alan R. Liss Inc., New York, pp. 51-136.

Trinkaus, E., 1988. The evolutionary origins of the Neandertals or, why were there Neandertals?, in: Trinkaus, E. (Ed), L'Homme de Néandertal, vol. 3, L'Anatomie, ERAUL, Liège, pp. 11-29.

Valladas, H., Mercier, N., Ayliffe, L., Falguères, C., Bahain, J.-J., Dolo, J.-M., Froget, L., Joron J.-L., Masaoudi, H., Reyss, J.-L., Moncel, M.-H., 2008. Radiometric dates for the Middle Paleolithic sequence of Payre (Ardèche, France). Quaternary Geochronology 3, 377-389.

Vialet, A., Modesto-Mata, M., Martinón-Torres, M., Martínez de Pinillos, M., Bermúdez de Castro, J.M., 2018. A reassessment of the Montmaurin-La Niche mandible (Haute Garonne, France) in the context of European Pleistocene human evolution. PLoS One 13, e0189714.

Weaver, T. D., 2009. The meaning of Neandertal skeletal morphology. Proceedings of the National Academy of Sciences of the USA 106, 16028-16033.

Weaver, T. D., Roseman, C. Stringer, C.B., 2007. Were Neandertal and modern human cranial differences produced by natural selection or genetic drift? Journal of Human Evolution 53, 135-145.

Weaver, T. D., Roseman, C. Stringer, C.B., 2008. Close correspondence between quantitative- and molecular-genetic divergence times for Neandertals and modern humans. Proceedings of the National Academy of Sciences of the USA 105, 4645-4649.

Zanolli, C., Martinón-Torres, M., Bernardini, F., Boschian, G., Coppa, A., Dreossi, D., Mancini, L., Martínez de Pinillos, M., Martín-Francés, L., Bermúdes de Castro, J.M., Tozzi, C., Tuniz, C., Macchiarelli, R., 2018. The Middle Pleistocene (MIS 12) human dental remains from Fontana Ranuccio (Latium) and Visogliano (Friuli-Venezia Giulia), Italy. A comparative high resolution endostructural assessment. PLoS ONE 13, e0189773.

Figure captions:

Figure 1 - Map of South-East France showing the location of Payre and other main Middle Palaeolithic sites in the region.

Figure 2 – TL and ESR-U/Th datings of the Payre sequence (from Valladas et al., 2008). Black stars indicate the location of human remains found at the site and the photograph of the Payre 15 mandible illustrates its position in the level Ga.

Figure 3 – The mandible Payre 15 in a) upper, b) lateral, c) posterior, d) anterior, e) lower and f) inner views. Scale in centimeters.

Figure 4 – 3D virtual surface model of Payre 15 after segmentation in a) occlusal, b) antero-medial and c) lateral views.

Figure 5 – Occlusal views of the lower P_4 and M_1.

Figure 6 - Bivariate plot of the mandibular corpus height at M_1 vs the bi-M_2 breadth of the mandible (after virtual reconstruction). MPH: European Middle Pleistocene hominins; EN: MIS 7-5e Early Neandertals; LN: MIS 5d-3 late Neandertals; EMH: African and SW Asian Early Modern Humans.

Figure 7- Principal Component Analyses of five mandibular linear measurements: mandibular corpus height and breadth at the symphysis (HS, ES) and at the M_1 (HM_1, M_1), bi-M_2 external width of the mandible after its virtual reconstruction (Bi-M_2W). a): PCA performed on the

raw dimensions. B): between-group PCA (bgPCA) performed on the Log Shape Ratios. MPH: European Middle Pleistocene hominins; N: MIS 7-3 Neandertals; EMH: African and South-West Asian Early Modern Humans.

Figure 8 –Principal Component Analysis of the Fourier descriptors of the nine first harmonics (PC1 and PC3).
MPH: European Middle Pleistocene hominins; N: MIS 7-3 Neandertals; EMH: African and South-West Asian Early Modern Humans; RMH: recent modern humans.

Figure 9 – Quantitative analysis of the M_1 roots. a) Principal component analysis of 5 root size variables (root length, 2√cervical plane area, 3√root stem volume, 3√root apex volume, 3√root pulp volume). b) Box and whisker plot of first molar root surface area. c) Reduced major axis regression of cervical plane area and root surface area for the M_1 sample. UMPH: European Middle Pleistocene hominins; N: MIS 7-3 Neandertals; EMH: African and South-West Asian Early Modern Humans; RMH: recent modern humans.

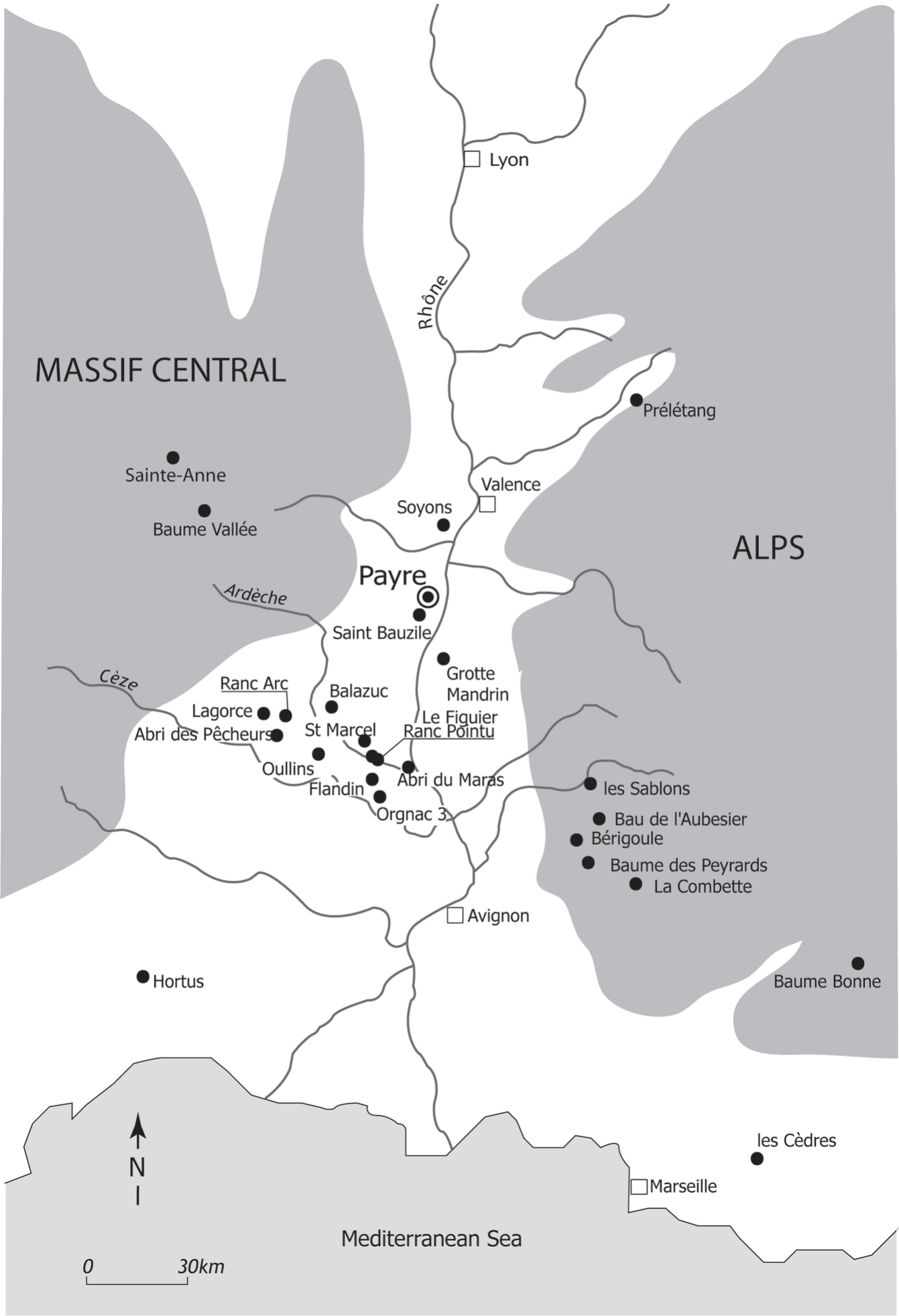
Lyon
Rhône
MASSIF CENTRAL
Prélétang
Sainte-Anne
Valence
Soyons
Baume Vallée
ALPS
Payre
Ardèche
Saint Bauzile
Grotte
Mandrin
Cèze
Ranc Arc
Balazuc
Lagorce
Le Figuier
Abri des Pêcheurs
St Marcel
Ranc Pointu
Oullins
Abri du Maras
Flandin
les Sablons
Orgnac 3
Bau de l'Aubesier
Bérigoule
Baume des Peyrards
La Combette
Avignon
Hortus
Baume Bonne
les Cèdres
N
Marseille
Mediterranean Sea
0
30km

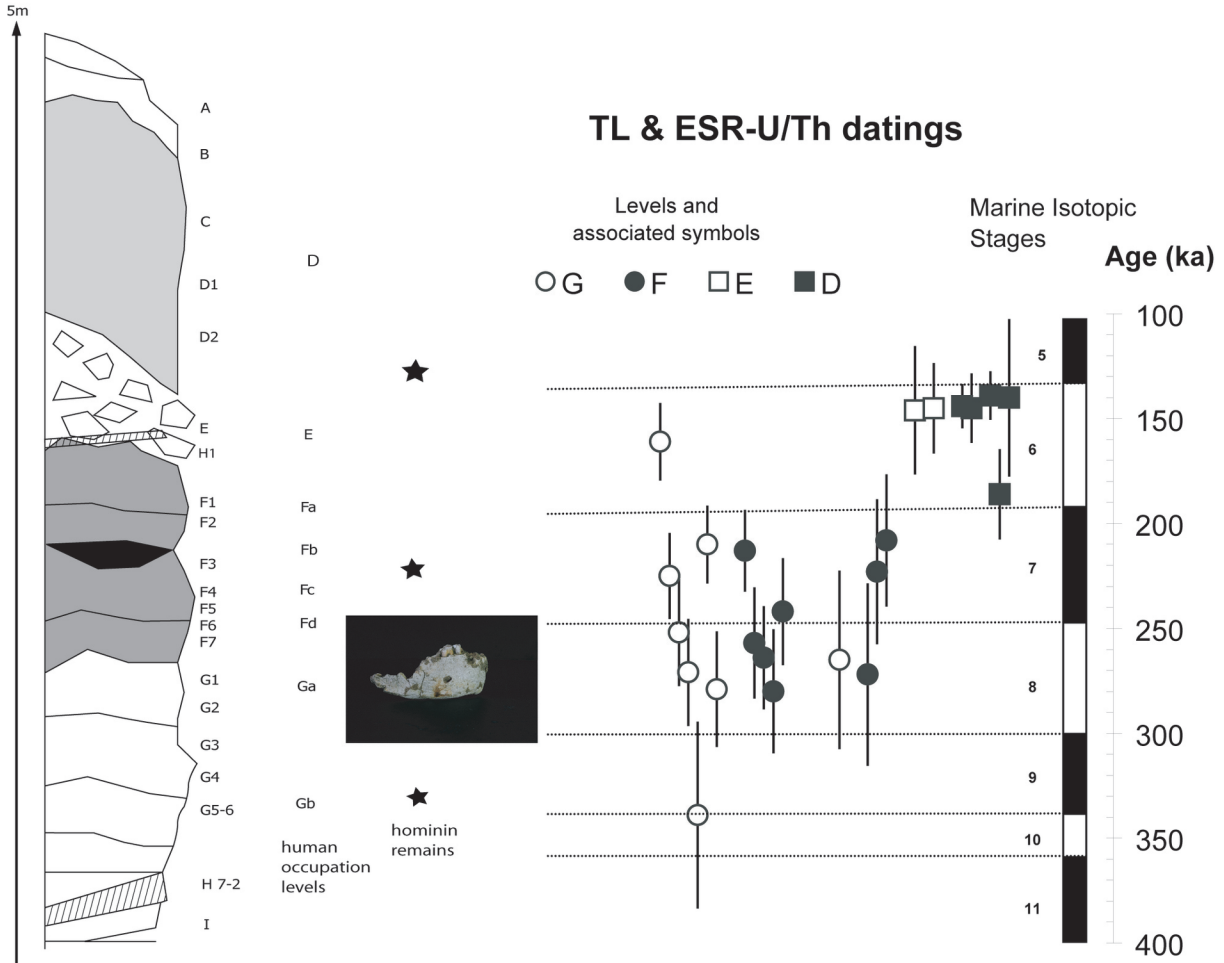
5m
A
B
C
D1
D2
E
H1
F1
F2
F3
F4
F5
F6
F7
G1
G2
G3
G4
G5-6
H 7-2
I
TL & ESR-U/Th datings
Levels and associated symbols
G
F
E
D
Marine Isotopic Stages
Age (ka)
100
150
200
250
300
350
400
5
6
7
8
9
10
11
D
E
Fa
Fb
Fc
Fd
Ga
Gb
human occupation levels
hominin remains

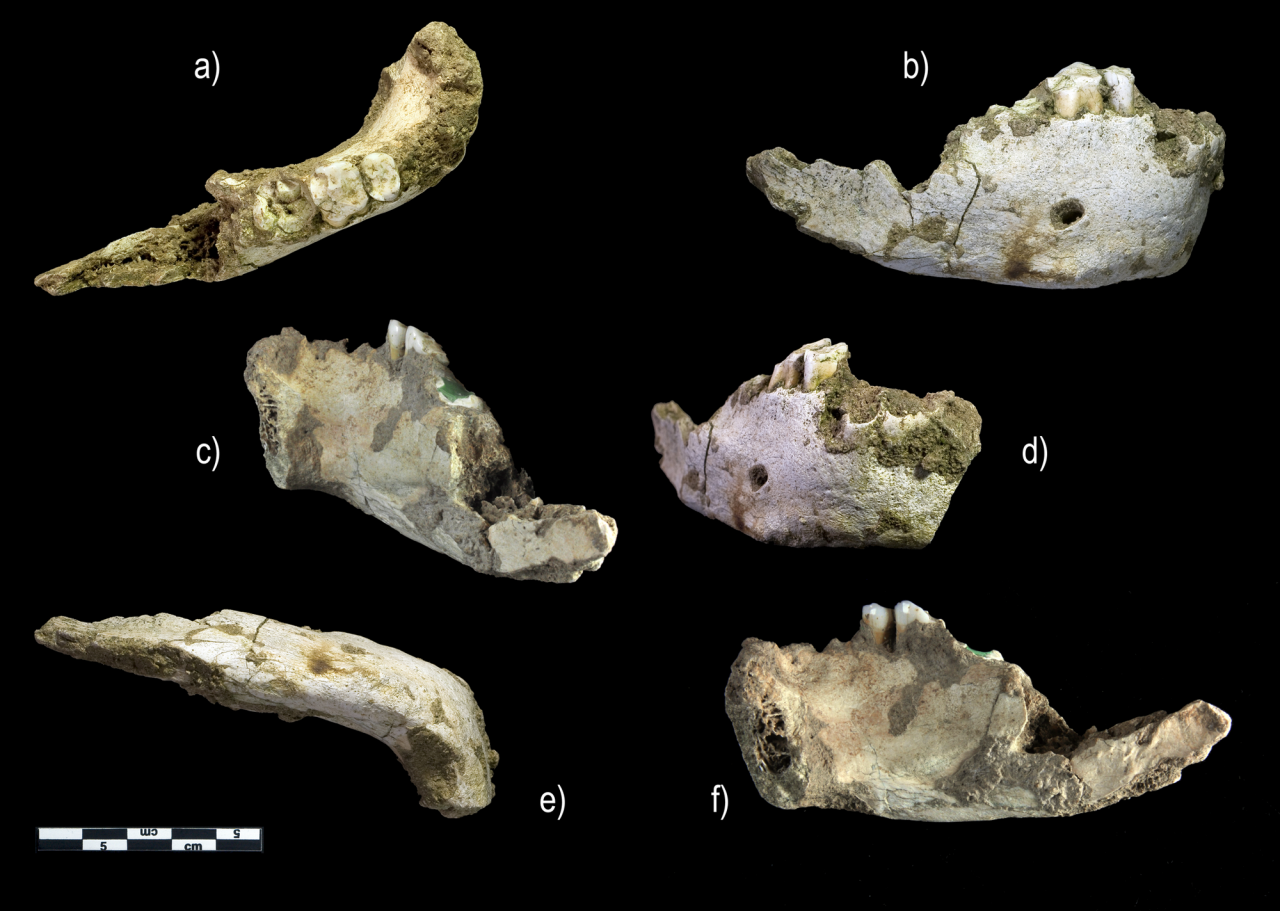
a)
b)
c)
d)
e)
f)
5
cm
5
cm

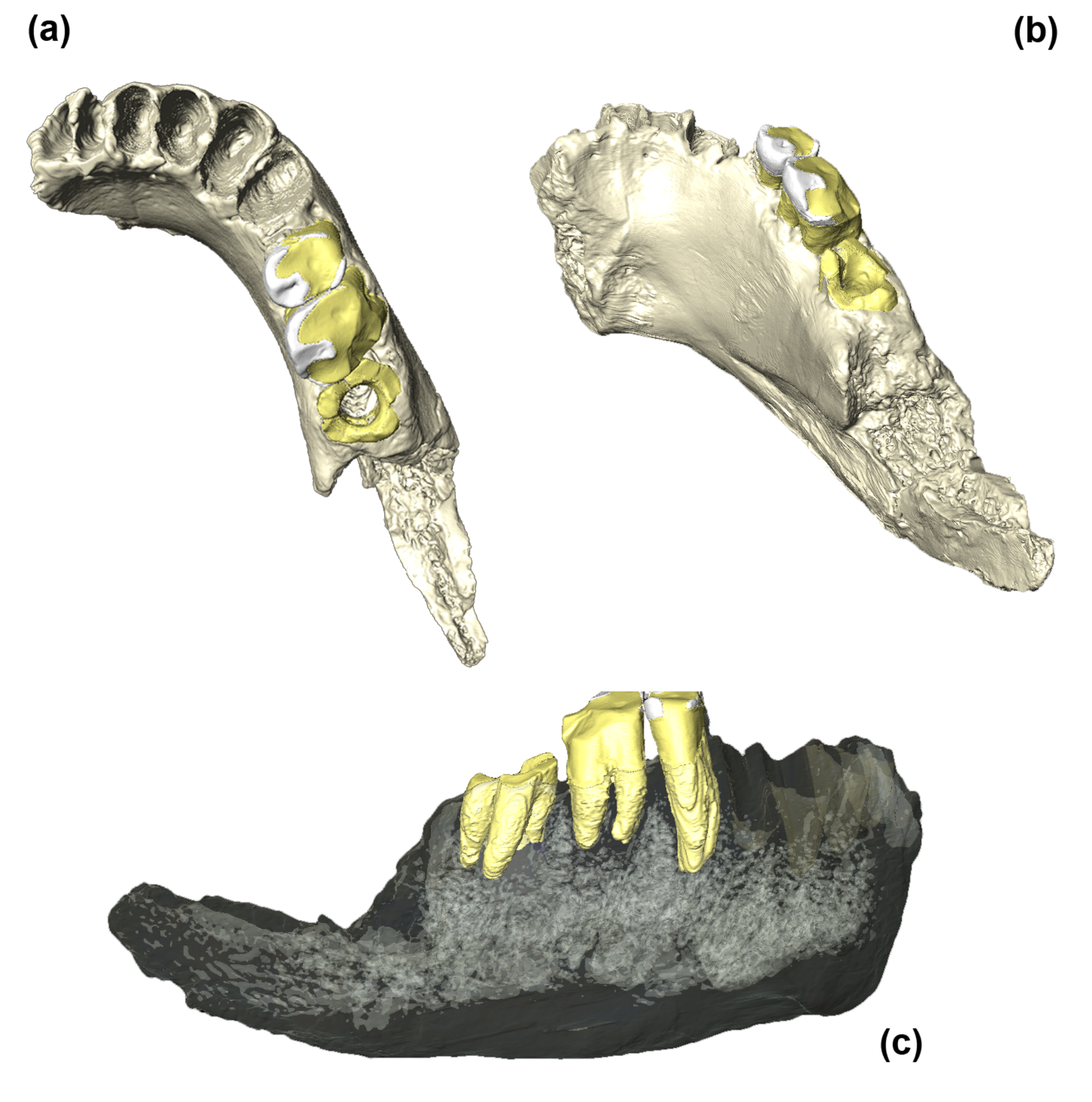
(a)
(b)
(c)


1 cm

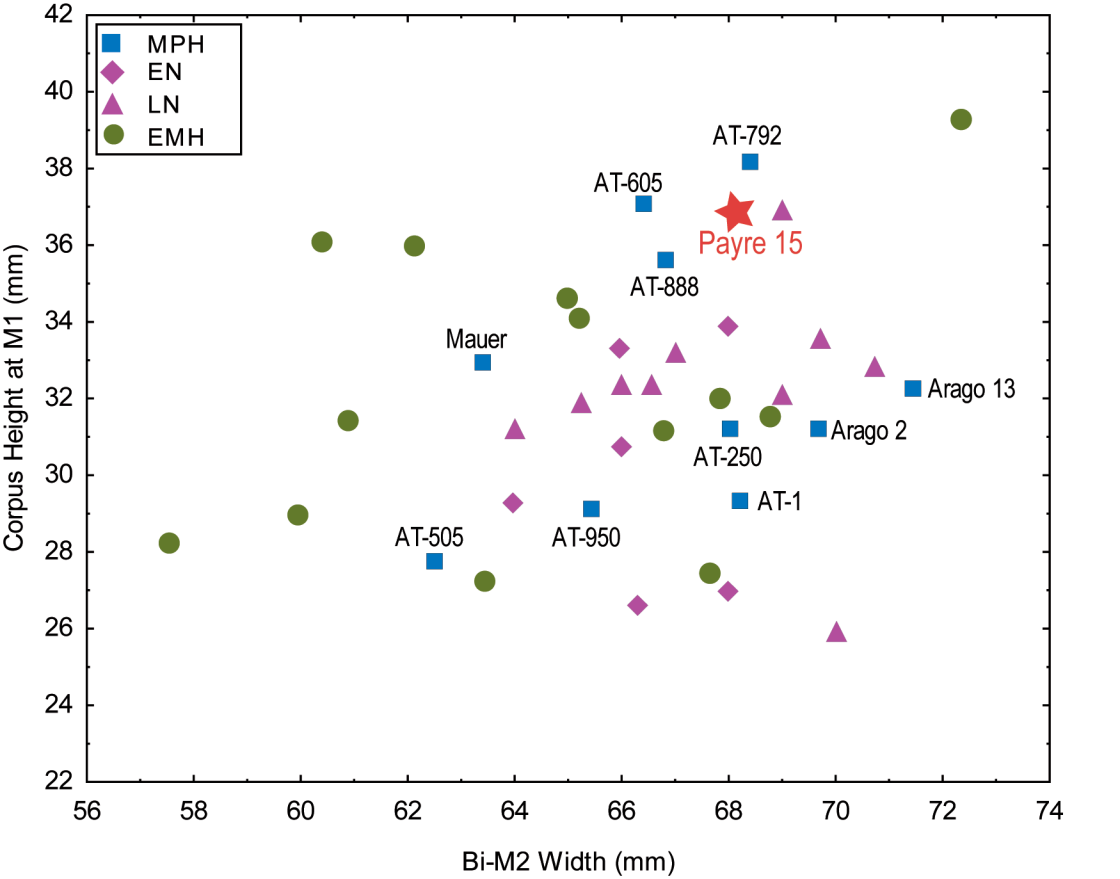
MPH
EN
LN
EMH
AT-792
AT-605
Payre 15
AT-888
Mauer
Arago 13
Arago 2
AT-250
AT-1
AT-505
AT-950
Corpus Height at M1 (mm)
Bi-M2 Width (mm)
42
40
38
36
34
32
30
28
26
24
22
56
58
60
62
64
66
68
70
72
74

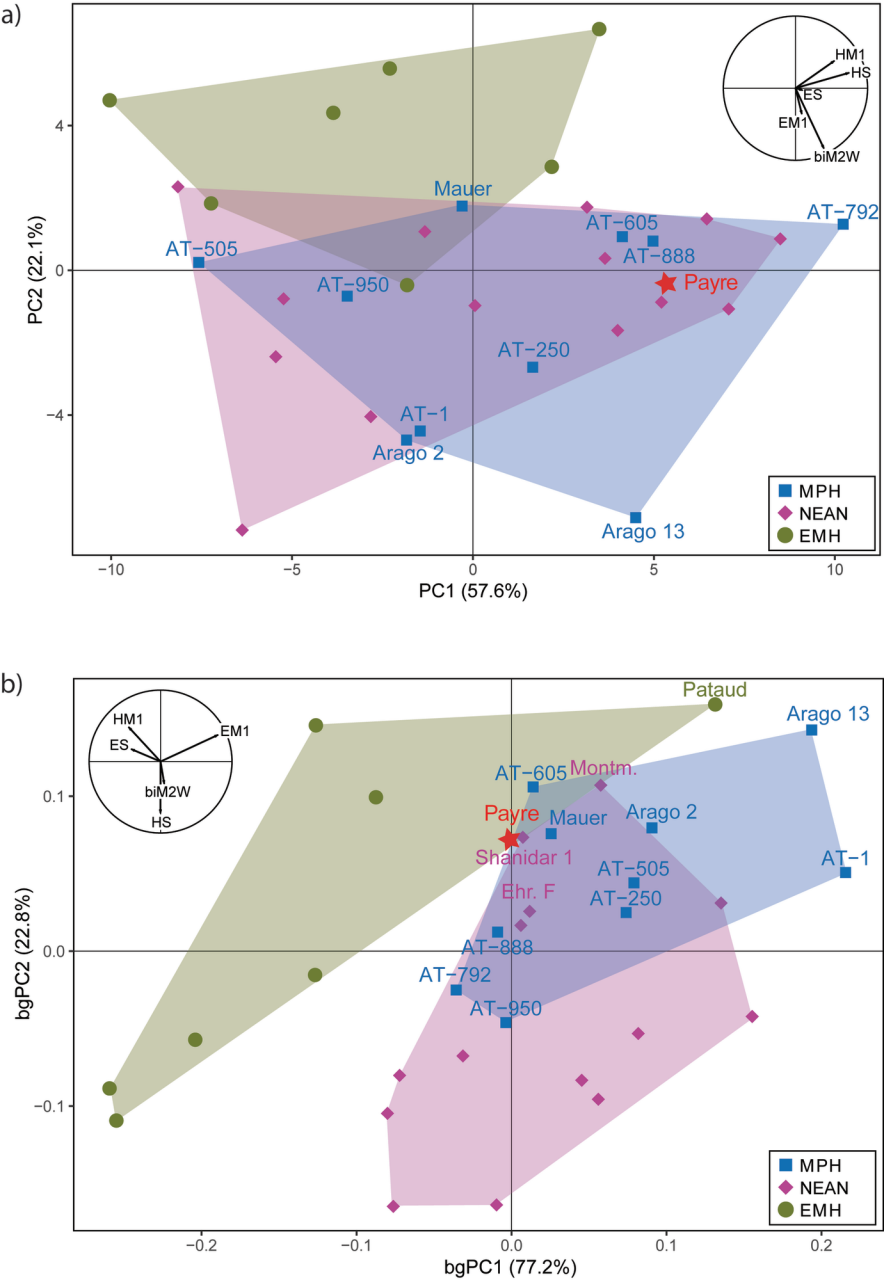
a)
HM1
HS
ES
EM1
biM2W
Mauer
AT−605
AT−792
AT−505
AT−888
AT−950
Payre
AT−250
AT−1
Arago 2
Arago 13
MPH
NEAN
EMH
PC2 (22.1%)
PC1 (57.6%)
b)
HM1
EM1
ES
biM2W
HS
Pataud
Arago 13
AT−605
Montm.
Payre
Mauer
Arago 2
Shanidar 1
AT−505
AT−1
Ehr. F
AT−250
AT−888
AT−792
AT−950
MPH
NEAN
EMH
bgPC2 (22.8%)
bgPC1 (77.2%)

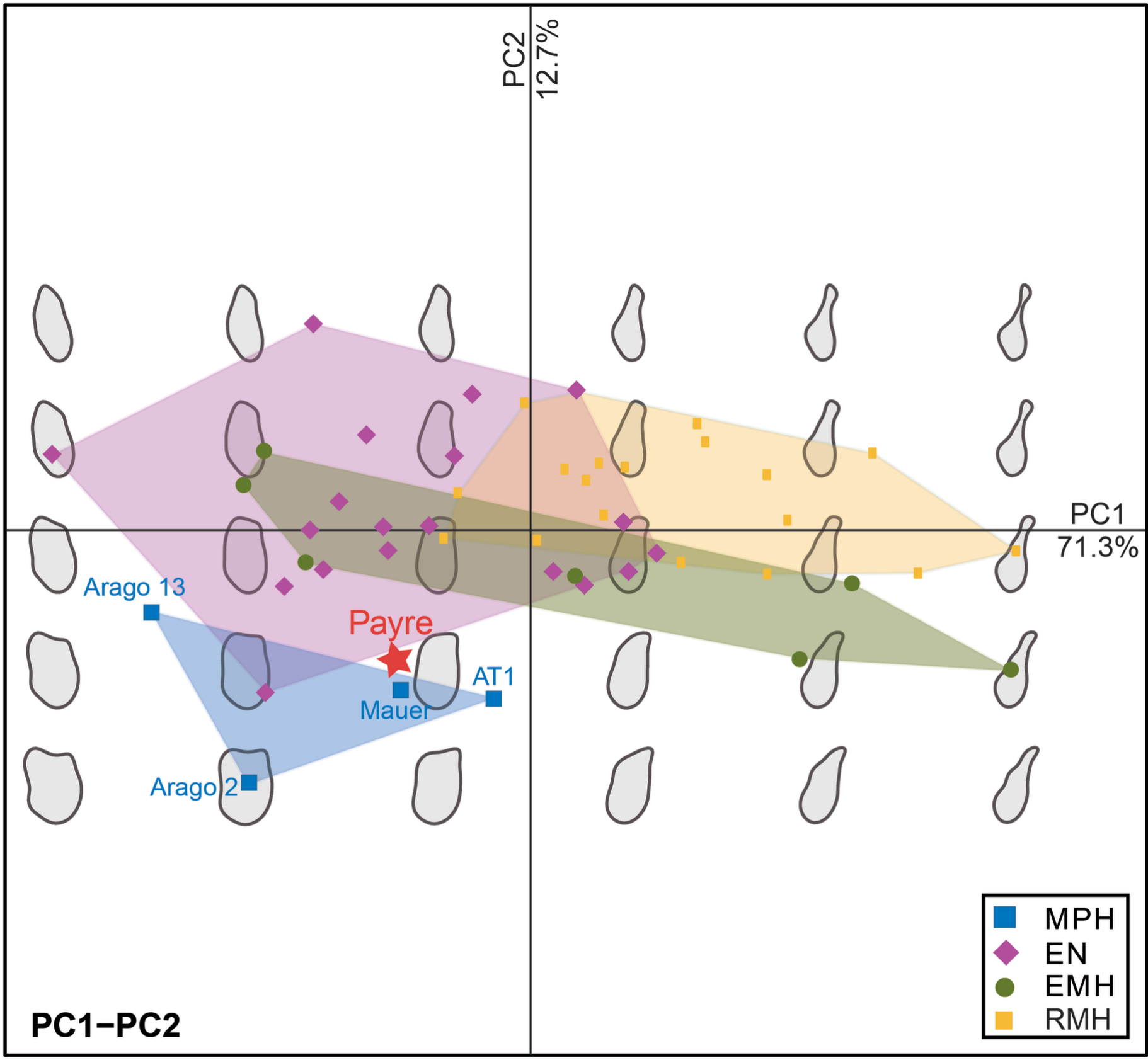
PC2
12.7%
PC1
71.3%
Arago 13
Payre
AT1
Mauer
Arago 2
MPH
EN
EMH
RMH
PC1–PC2

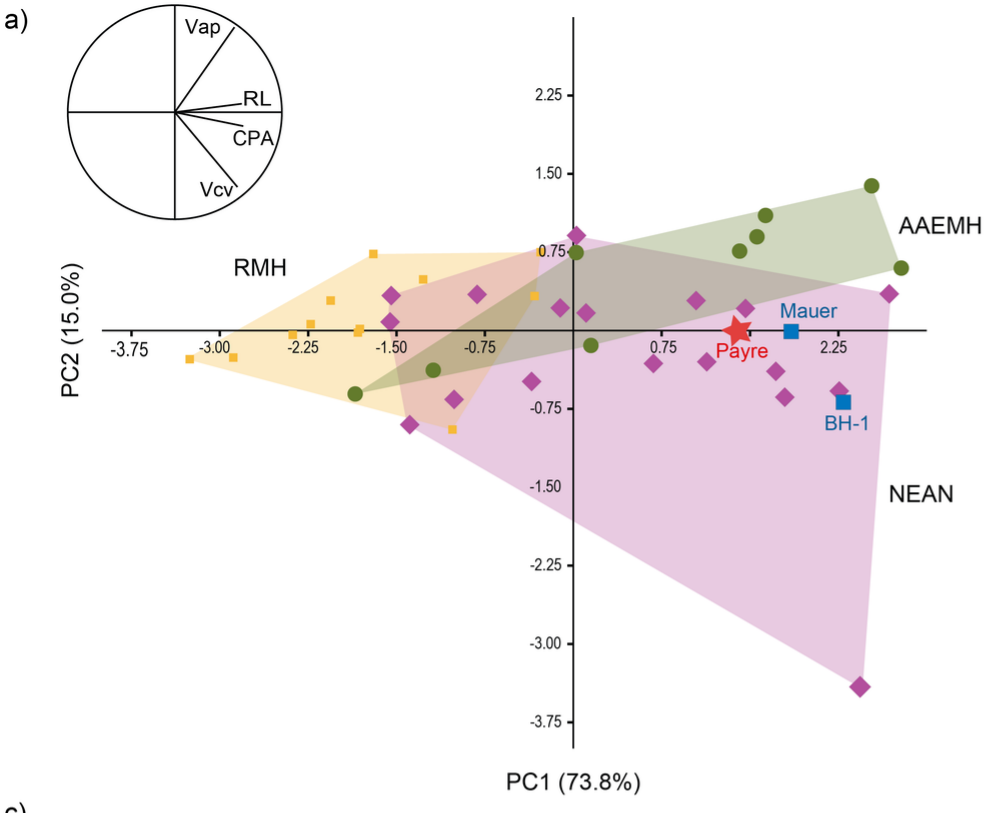
a)
Vap
RL
CPA
Vcv
RMH
AAEMH
NEAN
Mauer
Payre
BH-1
PC2 (15.0%)
PC1 (73.8%)
2.25
1.50
0.75
-0.75
-1.50
-2.25
-3.00
-3.75
-3.75
-3.00
-2.25
-1.50
-0.75
0.75
2.25

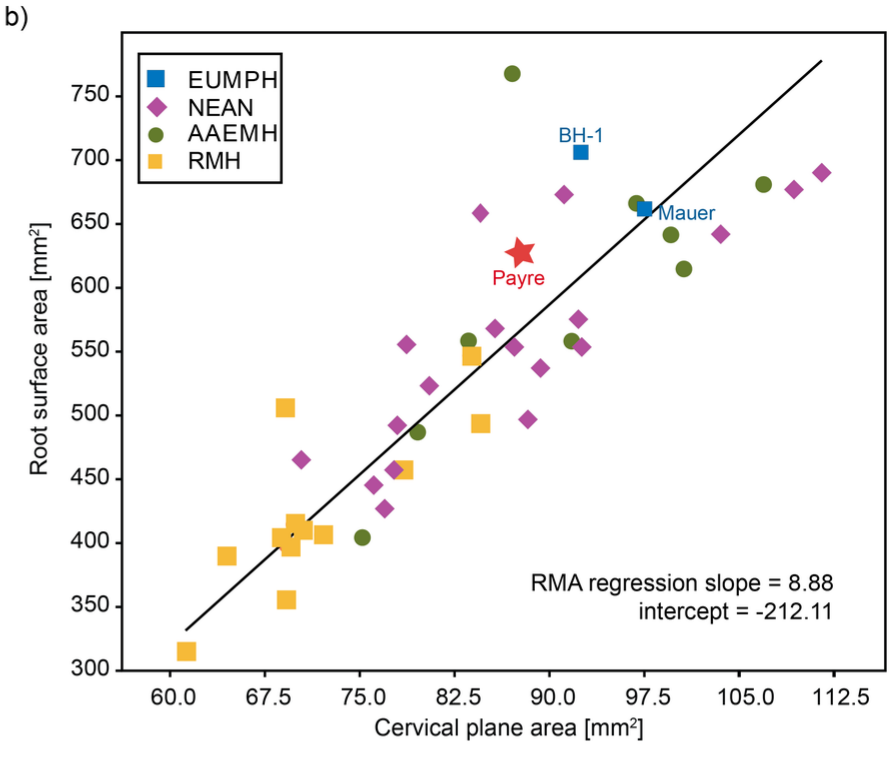
b)
EUMPH
NEAN
AAEMH
RMH
BH-1
Mauer
Payre
RMA regression slope = 8.88
intercept = -212.11
Root surface area [mm²]
Cervical plane area [mm²]
750
700
650
600
550
500
450
400
350
300
60.0
67.5
75.0
82.5
90.0
97.5
105.0
112.5

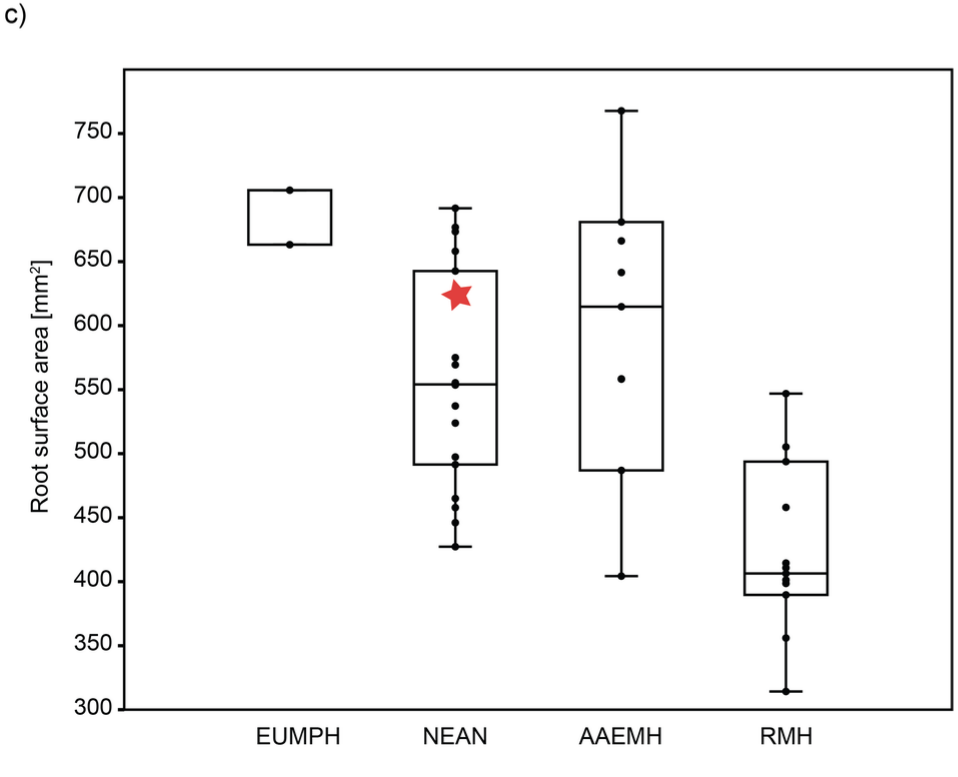
c)
Root surface area [mm²]
750
700
650
600
550
500
450
400
350
300
EUMPH
NEAN
AAEMH
RMH

Table 1 – Morphological features scored on the Payre mandible compared to frequency data for our comparative samples (number of individuals in bracket).[a]

		Character code[c]	Payre	MPH %	EN %	LN %	EMH
Foramen mentale single[b]		A	**X**	65 (10)	45,8 (12)	48,1 (26)	92,6 (27)
Foramen mentale location	<P4			0 (15)	0 (12)	0 (28)	17,2 (29)
	P4			6,7 (15)	12,5 (12)	5,4 (28)	74,1 (29)
	P4/M1			33,3 (15)	20,8 (12)	32,1 (28)	8,6 (29)
	≥M1	B	**X**	60 (15)	66,7 (12)	62,5 (28)	0 (29)
Prominentia lateralis location	M2			0 (12)	0 (10)	6,7 (15)	57,1 (21)
	M2/M3			29,2 (12)	30 (10)	6,7 (15)	40,5 (21)
	M3	C	**X**	70,8 (12)	70 (10)	86,7 (15)	2,4 (21)
Mentum osseum rank	**1**	D	**X**	80 (10)	22,2 (9)	13,6 (22)	0 (27)
	2-3			20 (10)	77,8 (9)	86,4 (22)	3,7 (27)
	4-5			0 (10)	0 (9)	0 (22)	96,3 (27)
Mylohyoid line pattern	**Diagonal**	E	**X**	67,9 (14)	77,8 (9)	100 (16)	74 (25)
	Low	F	**X**	92,3 (13)	33,3 (9)	12,5 (16)	4,3 (23)
	Medium/High			7,7 (13)	66,7 (9)	87,5 (16)	95,5 (23)
A-F Combination			**X**	**44,4 (9)**	0 (8)	0 (11)	0 (18)
A-D Combination			**X**	**55,6 (9)**	0 (9)	16,7 (12)	0 (19)

[a]Abbreviations as follows: MPH: pre-MIS 9 European Middle Pleistocene hominins; EN: Early Neandertals; LN: late Neandertals; EMH: Early modern humans (Pleistocene *Homo sapiens;* Africa, Middle East, Europe).

[b]See the text for a description of the morphological features and scoring procedure.

[c]The letters (A) to (F) refers to the morphological features that are combined in the two last lines of the Table.

Table 2 – Mandibular corpus metrics (in millimeters) and Adjusted-z-score (Azs) of the Payre measurements assessed for each comparative samples.[a]

		MPMH				Early Neandertals				Late Neandertals				EMH			
	Payre	**n**	**m**	**sd**	**Azs**	**n**	**m**	**sd**	**Azs**	**n**	**m**	**sd**	**Azs**	**n**	**m**	**sd**	**Azs**
HS	**35,7**	12	33,7	3,5	0,26	8	34,6	6,4	0,07	19	34,2	4,9	0,14	39	32,59	4,39	0,34
HP4	**35,8**	4	30,7	2,7	0,59	8	32,4	3,7	0,39	16	32,8	3,1	0,45	17	31,70	3,96	0,48
HM1	**36,8**	13	32,4	3,2	0,62	9	31,3	3,6	0,67	15	31,4	3,1	0,81	13	31,53	3,89	0,60
HM2	**35,6**	3	30,5	1,1		8	30,0	2,8	0,83	15	30,7	2,9	0,79	15	29,32	3,95	0,72
ES	**16,2**	12	15,4	1,8	0,22	7	15,3	1,8	0,20	16	15,2	1,2	0,40	31	15,31	1,95	0,22
EP4	**17,3**	5	16,9	3,0	0,05	8	15,9	1,4	0,42	14	14,7	1,2	1,02	27	12,70	2,02	1,09
EM1	**16,7**	12	16,6	2,1	0,02	9	15,5	1,1	0,47	16	14,8	1,4	0,61	23	14,07	2,33	0,53
EM2	**17,5**	3	18,8	4,4		8	15,4	1,0	0,87	16	15,5	1,4	0,70	26	14,95	2,52	0,48
INDS	**45,5**	12	45,8	4,5	-0,04	7	43,6	7,9	0,10	14	43,7	5,1	0,16	29	46,56	7,86	-0,06
INDP4	**48,3**	4	57,0	7,8		7	49,8	6,0	-0,10	11	44,9	4,9	0,31	21	39,39	9,09	0,46
INDM1	**45,3**	12	51,6	7,3	-0,40	9	50,0	5,0	-0,40	10	47,1	6,0	-0,13	16	45,10	8,93	0,01
INDM2	**49,3**	3	62,0	17,0		8	51,5	4,8	-0,20	13	50,6	6,3	-0,10	13	47,06	10,86	0,09
BiM2B	**68,1**	10	67,0	2,7	0,18	6	66,4	1,5	0,46	11	67,8	2,2	0,06	18	64,89	4,37	0,34

[a]Abbreviations as follows: MPH: European Middle Pleistocene Hominins; EMH: Early modern humans (Pleistocene *Homo sapiens*, Africa; Middle East, Europe). HS-HM2 and ES-EM2: height and breadth of the corpus at the symphysis and below the P_4, M_1 and M_2. INDS-INDM2: robusticity indices at the symphysis and below the P_4, M_1 and M_2. BiM2B: bi-M2 breadth.